Available online at www.sciencedirect.com
ScienceDirect
Coordination Chemistry Reviews 251 (2007) 1931–1950
COORDINATION CHEMISTRY REVIEWS
www.elsevier.com/locate/ccr

Review

Engineering of molecular architectures of β-diketonate precursors toward new advanced materials☆

Guglielmo G. Condorelli, Graziella Malandrino, Ignazio L. Fragalà *

Dipartimento di Scienze Chimiche, Università di Catania, and INSTM, UdR Catania, Viale A. Doria 6, I-95125 Catania, Italy

Received 17 January 2007; accepted 19 April 2007
Available online 24 April 2007

Contents

Abstract

Metal complexes bearing linked hexafluoroacetylacetonates and ancillary Lewis ligands, have found wide interest as precursors for metal-organic chemical vapor deposition (MOCVD) since their first description in 1991. The relationships involving their molecular architectures, mass transport properties, decomposition mechanisms of both alkaline- and rare-earth metal precursors are compared to fluorine-free β-diketonates. The perspectives of applications to MOCVD processes of a large range of advanced materials in thin film forms are discussed in detail. The effects due to the nature of the β-diketonate moiety as well as of the ancillary ligand on mentioned properties are discussed in detail.

Keywords: MOCVD; Alkaline-earth; Rare-earth; Adducts; Decomposition mechanisms; Thin films

1. Introduction

The development of novel and increasingly demanding materials requires challenging synthetic approaches ultimately suited for large scale fabrication of materials with specifically designed properties. Among the materials most studied over the last two decades have been those with particular electrical properties such as high-k dielectrics and ferroelectrics [$(Ba,Sr)TiO_3$ (BST), $SrBi_2Ta_2O_9$ (SBT), $SrTiO_3$] or high critical temperature (HTc) superconductors [$La_{2-x}Ba_xCuO_{4+\delta}$ [1], $YBa_2Cu_3O_{7-\delta}$ [2], $Bi_2Sr_2Ca_{n-1}Cu_nO_x$ [3], $Tl_mBa_2Ca_{n-1}Cu_nO_{2n+m+2}$ (where for $m = 1$, $n = 1$–5 and for $m = 2$, $n = 1$–4) [4]. In both cases a similar complex mixed oxide framework is present, which is based on a perovskite-type structure. The fabrication of these systems is

☆ Based on a keynote lecture presented at the 37th International Conference on Coordination Chemistry, 13–18 August 2006, Cape Town, South Africa.

* Corresponding author. Tel.: +39 095 336578; fax: +39 095 580138.
E-mail address: lfragala@dipchi.unict.it (I.L. Fragalà).

0010-8545/$ – see front matter © 2007 Elsevier B.V. All rights reserved.
doi:10.1016/j.ccr.2007.04.016

not very easy and requires well optimized reproducible synthetic routes. The success of potentially useful synthetic approaches, ranging from vapor- to liquid-phase routes, mostly depends on the properties of molecular precursors since their nature and architectures both drive the quality of materials. Nevertheless, relationships between the precursor molecular architectures and their properties still remain a challenge in the arena of materials science.

In this context, metal-organic chemical vapor deposition (MOCVD) has proved a great technique due to the use of simplified apparatus, lower deposition temperatures, the capability to coat complex shapes, the possibility to produce chemically complex systems and the adaptability to large scale processing [5]. This technique, in addition, is well suited for simultaneously coating both sides of substrates, whilst line of sight physical vapor deposition (PVD) techniques require sequential deposition steps for each of the two sides. Nevertheless, the quality of any MOCVD process crucially depends on the apparatus as well as on prerequisites of adopted precursors. Thus, reproducible results are always associated with a careful control of operational deposition parameters and, even more importantly, with the use of highly pure precursors with clean decomposition pathways and constant mass-transport properties.

Fundamental prerequisites of source precursors for any MOCVD process are thermal stability, sufficient and stable evaporation and good delivery properties under process conditions.

Metal β-diketonates $M(RCOCHCOR)_x$ (where R = alkyl, aryl, etc.) are amongst the most widely studied coordination compounds and have adequate characteristics in terms of mass transport properties [6]. In particular, group II metal β-diketonates often match the required properties for MOCVD processes and have found wider applications than metal alkoxides due to their generally higher volatilities, improved chemical stabilities and better mass-transport properties. They were first tested as MOCVD sources [7] and, therefore, they are usually referred as "first generation" precursors. For example, $Sr(tmhd)_2$ (Htmhd = 2,2,6,6-tetramethyl-3,5-heptanedione) represents to date the most used precursor for MOCVD production of Sr-containing materials such as BST, SBT, $SrTiO_3$ [8–12]. Nevertheless, despite its widespread use, this source suffers from certain drawbacks such as poorly reproducible syntheses, side decompositions and finally, a strong tendency to be coordinated by water and donor solvents [13,14]. Due to the large size and to the strong polarity of the alkaline earth metal centre, the group II metal β-diketonate complexes can be oligomeric or polymeric and hence species with low volatility. For example $[Sr(tmhd)_2]_3$ is a trimer with 3 six-coordinate Sr atoms in a distorted octahedral environment [15]. Moreover, side decomposition processes of metal β-diketonate precursors often result in carbon contaminations incorporated in oxide films grown by MOCVD [16,17].

A similar behavior has been observed for the Ca and Ba homologues, elements widely present in the HTc superconducting materials. In particular, problems associated with Ba are much more pronounced due to the larger ionic radius of this metal compared to the other alkaline earth metals.

Analogously, the conventional, "first generation", rare earth element precursors, such as $Ln(tmhd)_3$ have shown several drawbacks, essentially associated with the large amount of residue left in commercial evaporators/bubblers and to the poor stability to the atmosphere [18]. This behavior may be due, also in this case, to un-saturation of inner coordination spheres that opens-up routes for an easy polymerization or reaction either with donor solvents or nucleophilic impurities (such as water) that ultimately lead to low volatile polynuclear clusters or involatile oxo- or hydroxo-complexes [19].

This consideration prompted investigations in the 1990s into new suited metal complexes with coordination spheres capable of (i) inhibiting oligomerization and water coordination processes and (ii) improving the thermal stability, volatility and mass transport properties. A combined use of fluorinated β-diketonate arrays and of ancillary coordinated polyethers provided monomeric, volatile and thermally stable alkaline-earth metal sources, called "second-generation" precursors [14,20–33]. A similar strategy has been applied to lanthanide ions yielding thermally stable, highly volatile and very promising "second-generation" lanthanide MOCVD precursors [34–54]. In a recent review [55] the volatility, thermal stability and mass transport properties of "second generation" $Ln(hfac)_3$glyme (Hhfac = 1,1,1,5,5,5-hexafluoro-2,4-pentanedione) adducts were widely investigated. Most of these exhibit improved properties, in terms of thermal stability and volatility, thus being of potential interest for applications as precursors in the MOCVD of lanthanide containing phases [44,48,56–59]. They are also well suited as single precursors for the synthesis of fluoride and oxyfluoride phases, appealing materials as host matrices for luminescent ions [38,41,54,60].

Herein, we report on the engineering of precursor molecular architectures with specific properties based on an *a priori* tailoring of the coordination environment. A variety of alkaline- and rare-earth metal β-diketonate complexes coordinated with neutral Lewis bases are considered. The relationships involving molecular architectures, thermal and transport properties, decomposition kinetics and mechanisms are discussed in relation to deposition of advanced materials. The effects due to the ancillary ligand on mentioned properties are discussed in detail.

Accordingly, this review is divided into two main sections. Section 2 addresses the tailoring of alkaline earth (Ca, Sr, Ba) β-diketonates for improved MOCVD of electroceramics oxides focusing on vaporization, mass transport properties and decomposition pathways of $Sr(tmhd)_2$pmdeta (pmdeta = pentamethyldiethylenetriamine) and $M(hfac)_2$tetraglyme (M = Sr, Ba) precursors during MOCVD experiments. Ferroelectric SBT films and double sided TlBaCaCuO superconducting films are reported as case studies of applications of $M(hfac)_2$tetraglyme precursors. Section 3 discusses engineering of rare earth precursors for multi-source MOCVD of functional oxides, focusing on decomposition pathways of second generation $La(hfac)_3$diglyme and classical $La(tmhd)_3$ and $La(tmod)_3$ (H-tmod = 2,2,6,6-tetramethyloctane-3,5-dione) sources during MOCVD processes. The *in situ* synthesis of superconducting $La_{2-x}Ba_xCuO_{4+\delta}$ thin film is reported as a case study of applications of the $La(hfac)_3$diglyme complex.

2. Tailoring of alkaline earth β-diketonates for improved MOCVD of electroceramic oxides

2.1. Vaporization properties

Adducts of fluorine-free as well as fluorinated β-diketonates with neutral ligands have often been proposed as group II metal sources for MOCVD routes. In both cases, the coordination of ancillary Lewis base ligands causes a better spatial shield of the metal center and saturates the inner coordination sphere thereby precluding polymerization and increasing the vapor pressure [14]. Therefore, as a fluorine-free source, $Sr(tmhd)_2L$ (L = pmdeta and tetraglyme) precursors represent suitable alternatives to classical β-diketonates and they can be efficiently used in MOCVD reactors if equipped with liquid delivery systems [61].

The efficiency of the sublimation processes can be evaluated using thermogravimetric analyses (TG). $Sr(tmhd)_2$pmdeta shows (Fig. 1) two mass losses in the 125–230 °C (weight loss 28%) and in the 230–290 °C (total residue left <1%) temperature ranges. The first step represents the depletion of the amine ligand while the second is indication of the sublimation of the $Sr(tmhd)_2$ fragment. Similar results have been reported for $Sr(tmhd)_2$(deta) (deta = diethylenetriamine), $Sr(tmhd)_2$(teta) (teta = triethylenetriamine) and $Sr(tmhd)_2$(tetraglyme) analogues. In all cases ligand dissociation occurs in the same temperature range [15,62]. Note that the $Sr(tmhd)_2$pmdeta sublimes in a lower temperature range (230–290 °C) than the parent $Sr(tmhd)_2$ (300–400 °C [15]; 240–400 °C [63]). There is therefore indication that the pmdeta amine ligand precludes oligomerization processes and favors volatilization [14,64]. Even more important, the $Sr(tmhd)_2$ leaves a significant residue upon sublimation [11,65] while the $Sr(tmhd)_2$pmdeta shows a clean evaporation without further side decomposition in the 230–280 °C range as indicated by the linear trend of the logarithmic plot of the vaporization rate versus $1/T$ (Fig. 1, inset).

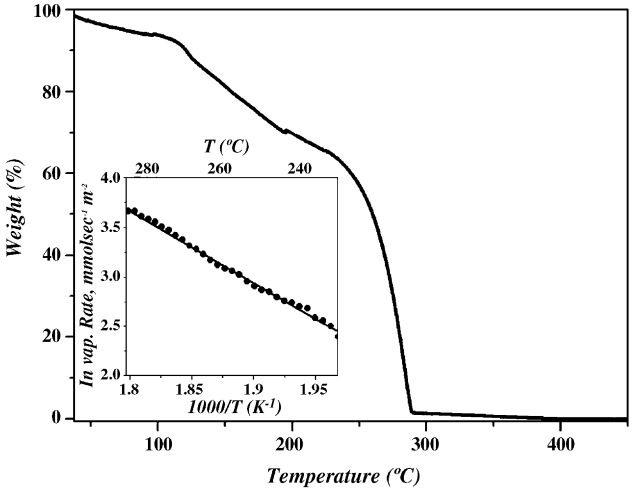

Fig. 1. TG curve of $Sr(tmhd)_2$pmdeta in inert atmosphere in the 30–450 °C temperature range (heating rate 5 °C/min). The inset shows the atmospheric pressure TG vaporization rate as a function of temperature in the 230–280 °C temperature region [68].

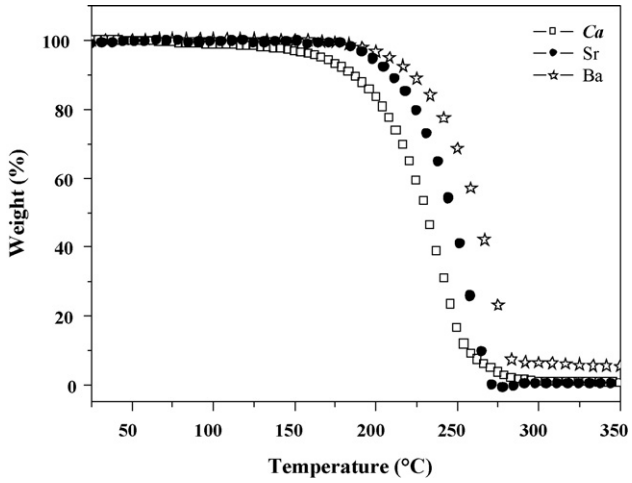

Fig. 2. TG profiles of Ba(hfac)$_2$tetraglyme, Sr(hfac)$_2$tetraglyme and Ca(hfac)$_2$tetraglyme under N_2 flow in the 25–350 °C temperature range at 760 Torr (heating rate 5 °C/min).

Turning to fluorinated β-diketonates, alkaline-earth hexafluoroacetylacetonate precursors have improved volatilities [66] and, once coordinated with ancillary Lewis bases such as polyethers, possess even better properties in terms of stability upon sublimation and mass transport. In particular the first adduct of the M(hfac)$_2$L family (the Ba(hfac)$_2$tetraglyme) was reported by Meinema et al., in 1991. This adduct has been widely applied analogously to the Sr and Ca homologues to MOCVD processes due to its excellent thermal properties. In fact the TG data of M(hfac)$_2$tetraglyme indicate superior thermal stability and great volatility under atmospheric and low pressure conditions [27]. There is evidence that sublimation occurs in a single step independently from the operational pressure values used in the experiments including atmospheric pressure (Fig. 2).

The excellent mass transport properties of these adducts become evident in the Arrhenius relationships in the 100–150 °C range (Fig. 3). It is interesting to observe that the Ca(hfac)$_2$tetraglyme precursor shows an apparent vaporization enthalpy ΔH_{vap} of $69 \pm 2\,kJ\,mol^{-1}$ with respect to $94 \pm 3\,kJ\,mol^{-1}$ and $87 \pm 3\,kJ \times mol^{-1}$ obtained

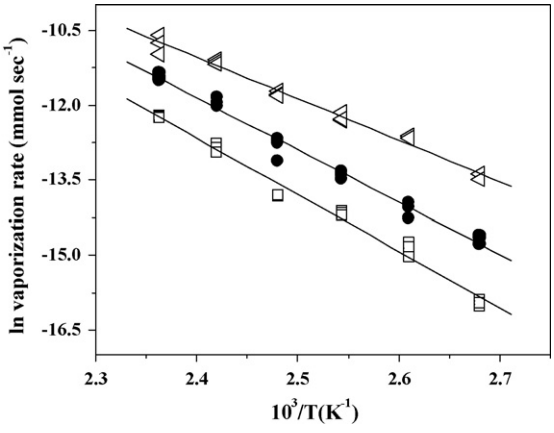

Fig. 3. Arrhenius diagram for vaporization of (□) Ba(hfac)$_2$tetraglyme, (●) Sr(hfac)$_2$tetraglyme and (△) Ca(hfac)$_2$tetraglyme.

for the Ba(hfac)$_2$tetraglyme and Sr(hfac)$_2$tetraglyme, respectively. The sizeable differences may be explained by different vaporization processes, namely sublimation of the solid Ba(hfac)$_2$tetraglyme (mp 153.6 °C), evaporation occurring from the molten Ca(hfac)$_2$tetraglyme (mp 94.2 °C) and an intermediate situation for the Sr(hfac)$_2$tetraglyme (mp 138.8 °C), that melts just within the investigated range. Such excellent thermal properties remain constant during several sublimation cycles in vacuo.

2.2. Mass-transport stability

FT-IR studies performed *in situ* [67,68] can provide further information on the precursor stability during mass transport in MOCVD processes. A typical apparatus for *in situ* analysis basically consists of an MOCVD hot-wall reactor interfaced with an FT-IR spectrometer (Fig. 4a).

These experiments show that the solid Sr(tmhd)$_2$L sources (L = pmdeta and tetraglyme) despite the favorable vaporization properties, are not suited for bubbler sublimation and transport into the MOCVD reactor. In fact, IR spectra point to detachment not only of the neutral L ligand but also of a much more massive demolition bringing about the free Htmhd as well as ketone by-products that form even at a temperature as low as 120 °C. This behavior has promoted the use of various liquid delivery systems to vaporize and transport Sr(tmhd)$_2$L precursors [61,68,69]. *In situ* FT-IR monitoring of direct liquid injector (DLI)-MOCVD (Fig. 4b) adopting Sr(tmhd)$_2$pmdeta dissolved in octane/decane solutions shows that liquid injection precludes a noticeable decomposition of the Sr(tmhd)$_2$ core during vaporization and transport into MOCVD reactors (up to 200 °C). Thus, the spectra of gas phase Sr(tmhd)$_2$pmdeta compared to those of both powders and octane/decane liquid solutions (Fig. 5) clearly show the bands (Table 1) of free neutral ligand at 1036 cm^{-1}, while bands at 1598 cm^{-1} typical of the coordinated tmhd remain unaffected [68,69]. This trend points to dissociation of the coordinated pmdeta and agrees well with the shape of the TGA plot.

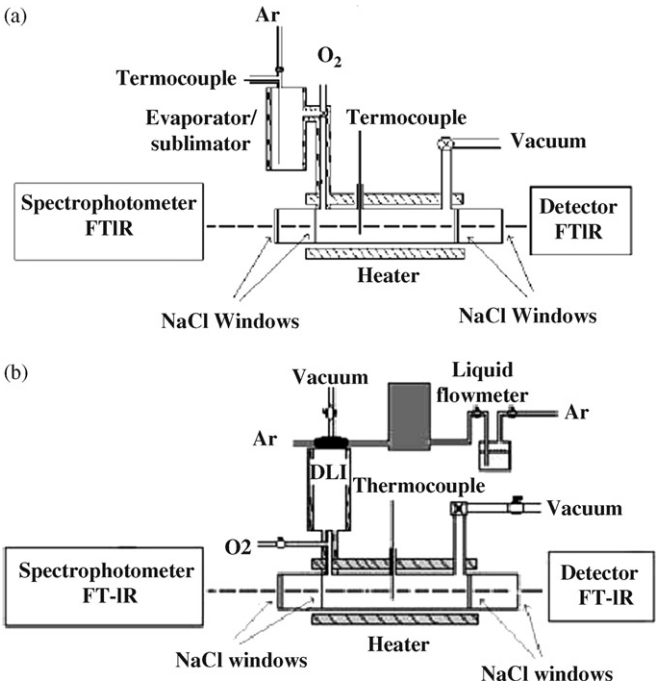

Fig. 4. MOCVD reactors equipped for *in situ* FT-IR spectroscopy. (a) Classical reactor with evaporation/sublimation bubblers [67] and (b) direct liquid injector (DLI)-MOCVD reactor [68].

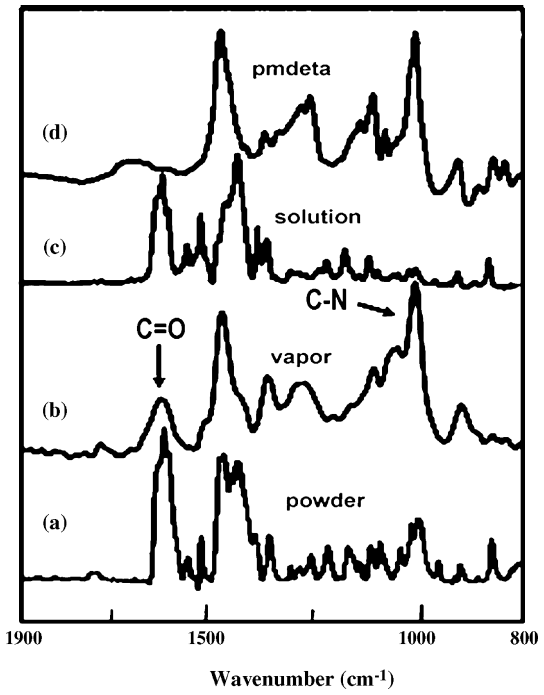

Fig. 5. Comparison of IR spectra of (a) Sr(tmhd)$_2$pmdeta powders, (b) Sr(tmhd)$_2$pmdeta in octane/decane solvent vaporized at 190 °C, (c) Sr(tmhd)$_2$pmdeta in octane/decane solution and (d) pure pmdeta. The absorption of the octane/decane has been subtracted from spectra (b) and (c) to clearly show the precursor bands [69].

Similarly Sr(tmhd)$_2$tetraglyme, vaporized from octane/decane solution, at 190 °C, shows a strong feature at 1130 cm^{-1}, typical of the C–O stretch of the tetraglyme ligand. Therefore, there is evidence that both Sr(tmhd)$_2$pmdeta and Sr(tmhd)$_2$tetraglyme precursors lose upon vaporization the ancillary ligands (pmdeta and tetraglyme, respectively) even though the Sr(tmhd)$_2$ core remains intact and acts as the true Sr precursor. To conclude, the coordination of an ancillary L ligand precludes oligomerization [14,64] and although it renders vaporization and storage more viable, it does not play a dominant role during the subsequent deposition process.

By contrast, the fluorinated Sr(hfac)$_2$tetraglyme precursor can be sublimed intact from the powder and related gas-phase FT-IR spectra (Fig. 6a) are similar to those of the powders (Fig. 6c) with no decomposition products visible [72]. Note, in this context, that a similar behavior was also observed in the case of other hexafluoroacetylacetonates glyme adducts [73]. In particular, Fig. 6b and d show similar FT-IR spectra for the gas phase and powders of the Ba(hfac)$_2$tetraglyme adduct.

Table 1
Typical IR bands of $Sr(tmhd)_2$pmdeta [68–71]

Wavenumber (cm^{-1})		Assignment of vibrations	Ligand frame
Powder	Gas		
2952, 2923, 2855	~2950–2850	ν(C–H)	tmhd/pmdeta
1598	1598	ν(C–O)	tmhd
1460	1440	ν_{as}(C–O) + ν(C–C) + δ(C–H)	tmhd/pmdeta
1356	1350 sh	$\delta(CH_3) + \delta$(C–H)	tmhd
1280	1270	ν(C–C) + $\nu[C–C(CH_3)_3]$	tmhd
1130	1128	$\nu[C–C(CH_3)_3] + \nu$(C–H)	tmhd
1080	1080	π(C–C) + $\pi(CH_3)$	tmhd
	1036	ν(C–N)	Free pmdeta
1024	–	ν(C–N)	pmdeta

ν: Stretching; δ: in-plane bending; π: out-of-plane bending; as: asymmetric.

2.3. Deposition processes from fluorinated and fluorine-free precursors

Fluorine-free as well as fluorinated β-diketonate adducts with neutral ligand have been proposed as Sr sources for efficient and reproducible deposition processes. In terms of mass transport stability, hexafluoroacetylacetonate adducts possess better properties than the related non-fluorinated adducts, even though their use, despite these advantages, has not been widely taken up in MOCVD processes of electroceramic oxides due to the presence of undesirable fluorine contaminants in "as deposited" films [17,74]. Such limitations find counterparts in other drawbacks encountered in depositions from fluorine-free sources whose films often show carbon contaminations [16,17]. The intriguing relations between the precursor nature, experimental conditions, decomposition pathways and film properties have been recently addressed [68,69,72,75].

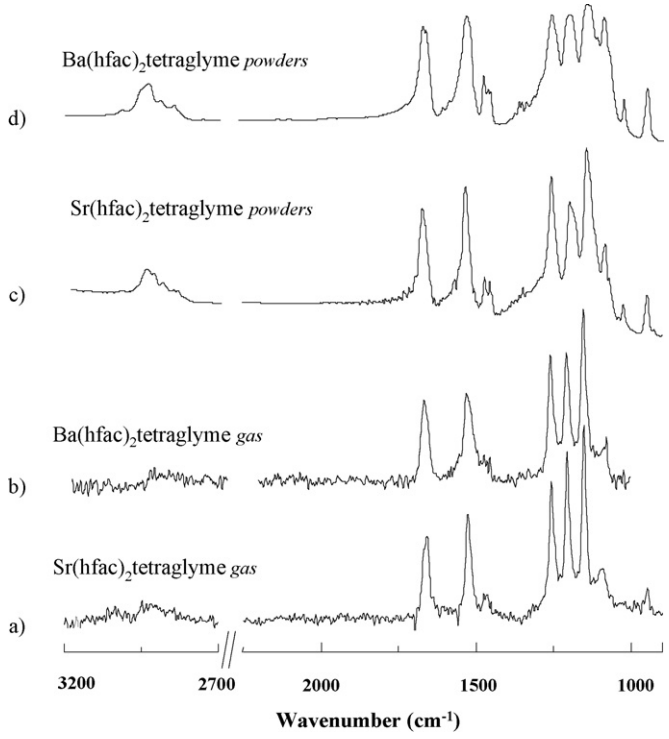

Fig. 6. *In situ* gas phase IR spectra of (a) Sr $(hfac)_2$tetraglyme and (b) $Ba(hfac)_2$tetraglyme. Spectra of (c) $Sr(hfac)_2$tetraglyme and (d) $Ba(hfac)_2$tetraglyme powders (KBr) have been added for comparison.

Typical DLI-MOCVD processes under Ar/O_2 with fluorine free $Sr(tmhd)_2$•pmdeta solutions [68] result in the formation of strontium carbonate films throughout the investigated deposition temperatures (300–500 °C). Fig. 7a shows the typical grazing incidence X-ray diffraction (GIXRD) pattern of films on Pt (deposited at 450 °C) indexed as $SrCO_3$ [76].

XPS depth profiles of the same films do not show evidence of nitrogen contamination in the entire investigated temperature range [68,69]. Moreover, the C 1s B.E. value (289.0 eV) after Ar^+ sputtering points to the presence of $SrCO_3$ [77–79]. Nevertheless, the O 1s feature splits in two bands in both bulk and film interface overlaying the substrate (Pt) as expected for the presence of $SrCO_3$ and SrO phases (at 531.8 and 528.1 eV, respectively).

The evolution of the shape of O 1s features at various deposition temperatures provides chemical information either of the bulk (Fig. 8a) or of the interface (Fig. 8b). Thus, the $SrO/SrCO_3$ ratio in the bulk (estimated from the ratio of the oxygen signals) is ~2:1 and does not depend on the temperature. By contrast, the SrO amount increases at the Pt-interface upon decreasing the deposition temperature [68,69]. These observations suggest that $SrCO_3$ forms by reactive adsorption of CO_2 by-product upon ligand oxidation [80,81]. Of course, smaller quantities of $SrCO_3$ are formed at lower deposition temperature, where decomposition to CO_2 is less efficient. This conclusion agrees well with FT-IR data (see the following section) that show that greater amounts of CO_2 are produced upon increasing the deposition temperature.

$SrO/SrCO_3$ films deposited at 450 °C are homogeneous and do not show well-detectable grains at lower precursor flow rates (Fig. 9a). Inhomogeneous films with very wide grains are, by contrast, observed upon increasing the precursor flow rate (Fig. 9b).

Typical MOCVD experiments adopting $Sr(hfac)_2$tetraglyme with Ar/O_2 mixtures (100 sccm[1]/500 sccm) result in the formation of randomly oriented SrF_2 films throughout the investigated

[1] sccm = standard cubic centimeter per minute.

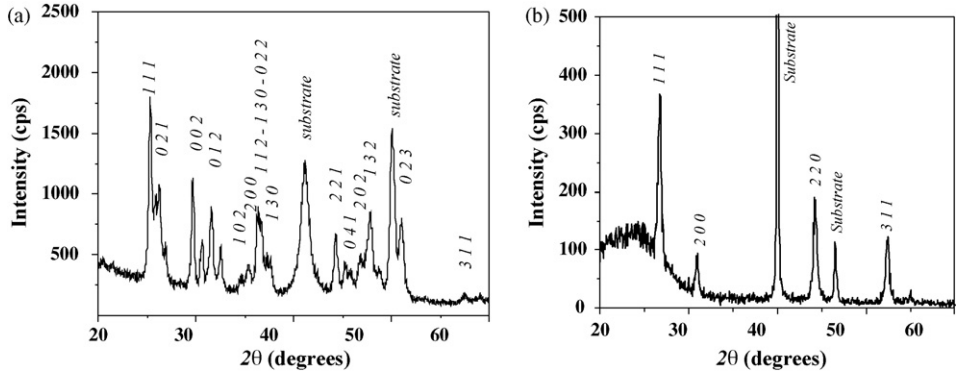

Fig. 7. Typical XRD patterns of (a) $SrCO_3$ phase obtained from $Sr(tmhd)_2$pmdeta [68] and (b) SrF_2 phase obtained from $Sr(hfac)_2$ tetraglyme [69]. Both films were deposited on Pt substrates.

deposition temperature range (250–500 °C) [72]. GIXRD patterns (Fig. 7b) of typical films show the (1 1 1), (2 0 0), (2 2 0) and (3 1 1) SrF_2 reflections and those of Pt (2 0 0) and (2 2 0) due to the Pt substrate.

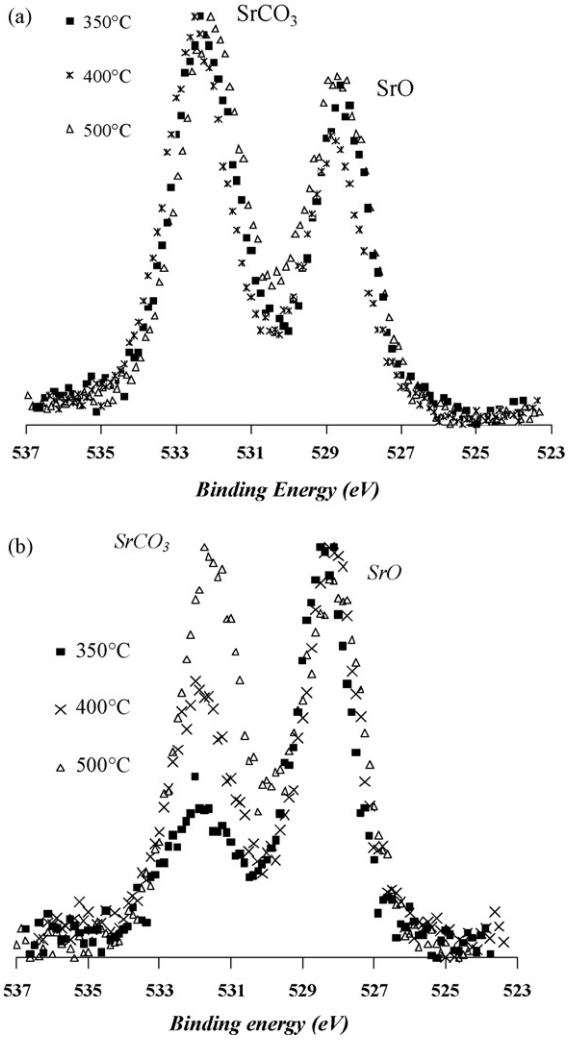

Fig. 8. XPS spectra of O 1s region of films obtained from $Sr(tmhd)_2$•pmdeta at several deposition temperatures (350–500 °C) and under Ar/O_2 flow: (a) bulk and (b) interface film/substrate (Pt) [68].

Similarly XPS data, namely the binding energy (B.E.) values of the Sr 3d spin–orbit doublet ($3d_{5/2}$ 133.9 eV and Sr $3d_{3/2}$ 135.6 eV) and the F 1s feature (683.9 eV), are consistent with SrF_2 [72,82]. Spectra of the surface show also some features due to ligand fragments containing CF_x groups (F 1s 688 B.E.) [82,83], which are no longer detectable after sputtering.

SrF_2 films deposited at low temperature (350 °C) have grains which are not-well defined in shape, with dimensions ranging from 50 to 300 nm (Fig. 10a). Higher temperatures (450 °C) result in grains with well-defined cubic and octahedral shapes (Fig. 10b) having larger average size (about 200–300 nm).

2.4. Decomposition pathways of precursors during MOCVD

FT-IR/MOCVD experiments are viable tools to investigate precursor decomposition pathways upon deposition.

Typical FT-IR/MOCVD experiments using fluorine-free $Sr(tmhd)_2$pmdeta solutions and adopting Ar/O_2 as transport/reacting gas indicate that, besides the ancillary ligand dissociation upon vaporization (see Sections 2.1 and 2.2), no significant decomposition of the $Sr(tmhd)_2$ core occurs below 300 °C (Fig. 11). Above this temperature, ligand demolition becomes apparent and the absorbance of the C=O stretching (1598 cm^{-1}) of the coordinated tmhd decreases and a new peak appears at 1720 cm^{-1}. The latter can be attributed to the C=O stretching of ketone by-products in the gas phase. The presence of ketones has often been observed in the decomposition of several metal β-diketonates [84–87]. At 500 °C, the band at 1598 cm^{-1} almost disappears and new IR modes associated with different by-products become evident. They consist of two bands centered at 2295 and 2163 cm^{-1} associated with CO_2 and CO molecules due to precursor decomposition.

Therefore, even though $Sr(tmhd)_2$pmdeta is not transported intact to the deposition zone due to the dissociation of the ancillary amine ligand, the $Sr(tmhd)_2$ core undergoes decomposition only above 300 °C. Various studies have indicated that this precursor suffers of a sequence of various bond ruptures, namely: (1) Sr–O → (2) C–$C(CH_3)_3$ → (3) C–C, (see Scheme 1 [65,88].

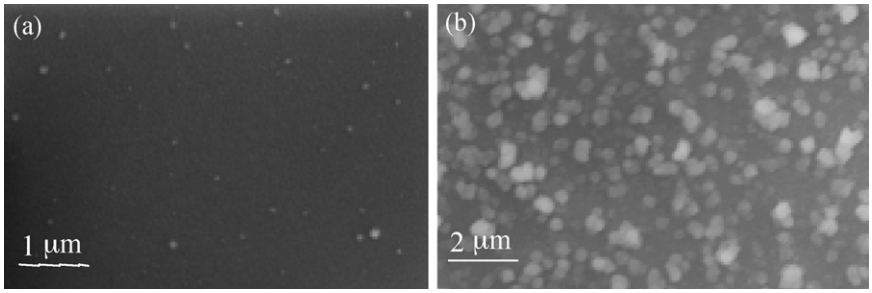

Fig. 9. SEM micrographs of films deposited from $Sr(tmhd)_2$pmdeta: (a) 2 g/h and (b) 4 g/h mass flow. [69].

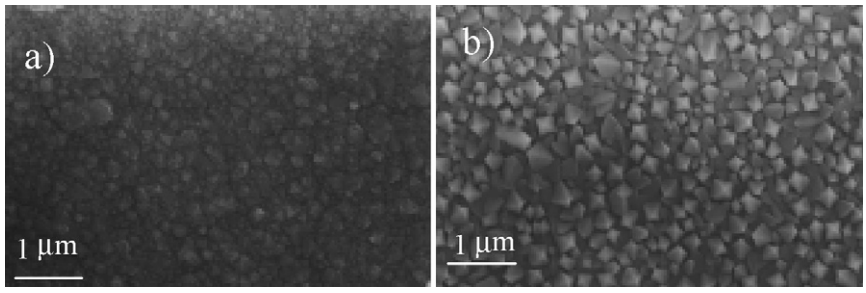

Fig. 10. SEM micrographs of films deposited from $Sr(hfac)_2$ tetraglyme: (a) 350 °C and (b) 450 °C [69].

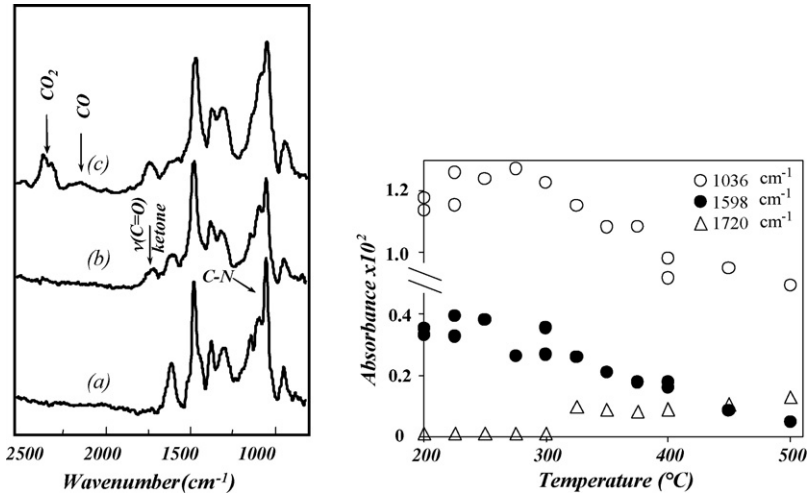

Fig. 11. Left: *in situ* FT-IR spectra of $Sr(tmhd)_2$•pmdeta after subtraction of solvent absorbances from the spectra of the gas phase (a) at 200–300 °C, (b) at 400 °C and (c) at 500 °C. Right: thermal dependence of IR absorbance of typical bands of $Sr(tmhd)_2$•pmdeta. (●) νC═O of $Sr(tmhd)_2$; (◯) νC–N of free pmdeta; (Δ) νC═O of ketone by-products [68].

The entire deposition pathway to $SrO/SrCO_3$ films evolves as sketched in Scheme 2. Significant evidence is, in fact, found in FT-IR spectra in terms of ketone by-products and of ligand oxidation/combustion by-products CO_2 and CO required to form $SrO/SrCO_3$ films. Higher temperature as well as higher precursor partial pressure favors the formation of CO_2 and in turn of $SrCO_3$ [68].

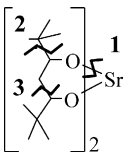

Scheme 1.

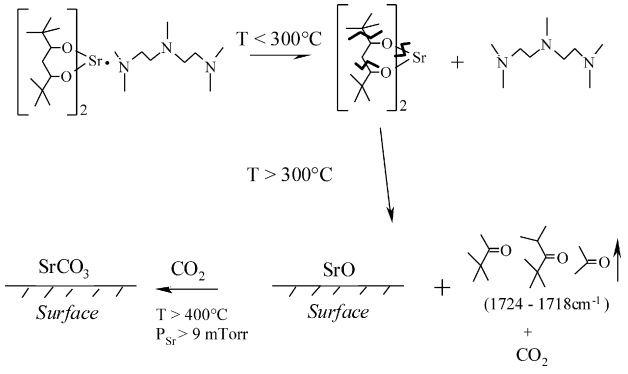

Scheme 2.

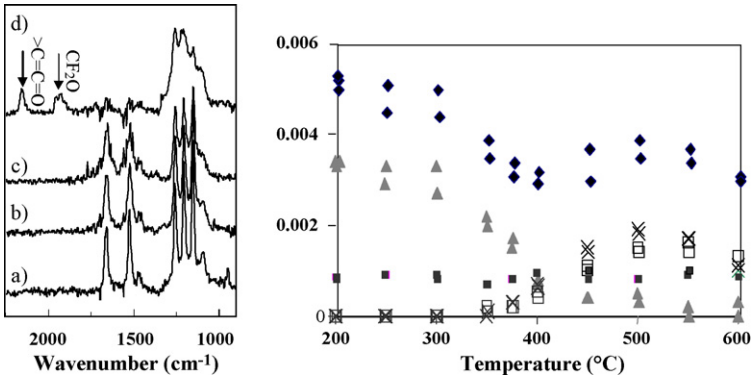

Fig. 12. Left: *in situ* FT-IR spectra of Sr(hfac)$_2$tetraglyme at various reactor temperatures in Ar/O_2 enviroment at (a) $T = 200\,^{\circ}C$; (b) $300\,^{\circ}C$; (c) $T = 350\,^{\circ}C$; (d) $T = 450\,^{\circ}C$. Right: thermal dependence of IR absorbance of typical bands of Sr(hfac)$_2$tetraglyme. (♦) 1256 cm^{-1} (Sr(hfac)$_2$tetraglyme, C–F stretch); (▲) 1660 cm^{-1} (Sr(hfac)$_2$tetraglyme, C=O/C=C stretches); (□) 1930 cm^{-1} (CF_2O); (×) 2150 cm^{-1} (C=C=O stretch, acylketenes); (■) 2900 cm^{-1}; (C–H stretches, tetraglyme) [72].

To conclude, mechanicistic studies provide suitable criteria for selection of deposition parameters (temperature and partial pressure) to obtain either SrO or $SrCO_3$ homogeneous films. Namely lower partial pressure or/and deposition temperatures favor SrO, whilst higher values of both parameters promote a fast and complete ligand decomposition with production of greater amount of CO_2 and, hence, of $SrCO_3$.

Fluorinated sources such as Sr(hfac)$_2$tetraglyme possess different decomposition pathways, which lead to SrF_2 films. Combined studies including ex situ film characterizations, *in situ* FT-IR analyses and kinetic studies [72] suggest that below $300\,^{\circ}C$ the precursor does not decompose in the gas phase (Fig. 12a and b) and that the deposition pathway involves the adsorption of the precursor on the film surface. Moreover, there is indication of a zero-order kinetics relative to the precursor concentration [72,89] as expected for a heterogeneous process. Note that temperatures above $300\,^{\circ}C$ increase the surface reaction rate and determine a faster consumption of the precursor compared to its feeding. Thus, bands at 1256–1220 cm^{-1} (C–F_x stretches) and at 1660 cm^{-1} (C=C/C=O stretches) associated with the hfac framework decrease in intensities, while maintaining the same shape (Fig. 12). It is worthy of note that modes at 2950–2850 cm^{-1} (C–H_x stretches) associated with either coordinated or free tetraglyme [67] do not show any intensity fall-off and that the observed trend of relative intensities of C–H_x stretches versus hfac features is tuned well with a surface process:

$$\text{Sr(hfac)}_2\text{tetraglyme (g)} \rightarrow \text{Sr(hfac)}_2\text{(ad)} + \text{tetraglyme (g)} \quad (1)$$

Therefore, adsorption causes the glyme dissociation (Eq. (1)) while a following surface reaction leads to fluorine transfer to the metal followed by the demolition of the β-diketonate framework (Scheme 3). The overall result is the formation of the SrF_2 film and of adsorbed CF_x containing species, consistent with the XPS data and IR analysis of desorbed species as well as with data reported for surface decomposition of closely related species [90–92]. Experiments on precursor thermal behavior under Ar [72] show that oxygen does not play a crucial role in the SrF_2 formation. Indeed, O_2 simply precludes carbon contaminations in the films since it governs oxidation of surface species.

Above $400\,^{\circ}C$ a different, homogeneous decomposition pathway of Sr(hfac)$_2$tetraglyme becomes dominant and IR spectra

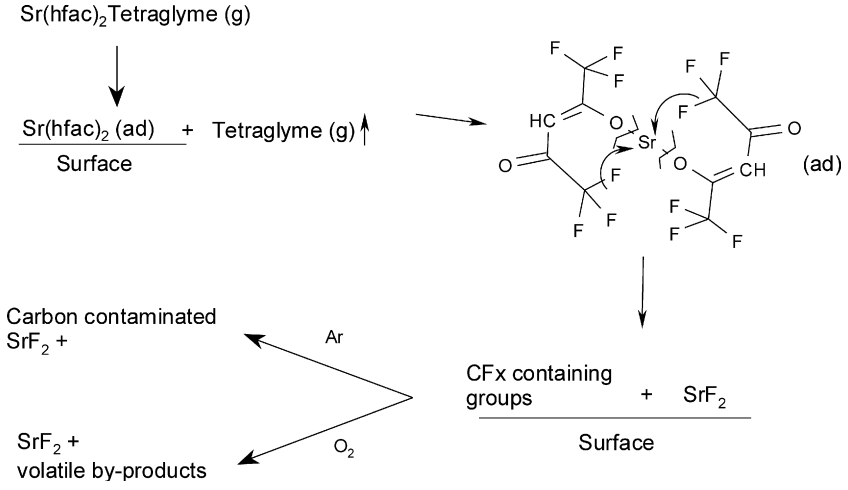

Scheme 3.

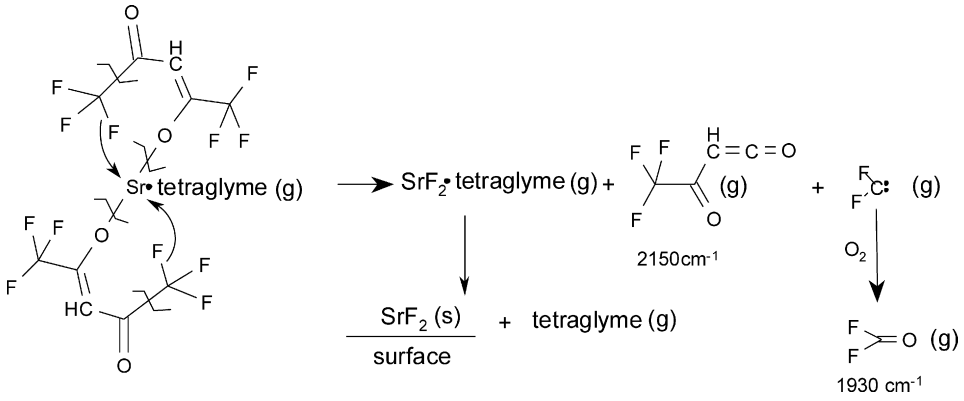

Scheme 4.

show much more complex features due to decomposition processes. IR absorptions due to precursor become considerably less intense (Fig. 12), whilst new features due to ketenes or acylketenes (>C=C=O) at 2150 cm^{-1} and CF_2O at 1930 cm^{-1} [93–95] become evident. Note, also, that similar by-products have been detected along MOCVD decomposition routes of similar fluorine containing hexafluoroacetylacetonate precursors [67]. This pathway probably involves intramolecular ($CF_3 \rightarrow Sr$) fluorine transfer through switching from bidentate to monodentate ligand coordination. The thermally activated opening of the chelate ring is not an unexpected issue since it has been proposed for closely related systems [47,96–98]. The proposed homogeneous pathway (Scheme 4), finally, leads to SrF_2 films with CF_2O and fluoroacylketens by products.

Closely comparable results have been found with Ba(hfac)$_2$-tetraglyme [73].

2.5. Preparation of ferroelectric $SrBi_2Ta_2O_9$ (SBT) films from fluorine containing precursors

MOCVD fabrication of $SrBi_2Ta_2O_9$ (SBT) ferroelectric films for new, non-volatile ferroelectrics memory applications (NVFeRAM), has been extensively investigated because of the advantages of MOCVD in terms of higher step coverage [99–101]. A suitable choice of a good set of metal-organic source precursors often remains the major challenge. The most used strontium precursors consist of fluorine-free Sr β-diketonates often coordinated with neutral ligands (polyethers and polyamines). Several studies have reported on the kinetics of multi-component SBT depositions using fluorine-free precursor systems such as $Bi(CH_3)_3$–$Sr[Ta(OC_2H_5)_6]_2$ [102], $Bi(C_6H_5)_3$–$Sr[Ta(OC_2H_5)_6]_2$ [103] and Sr(tmhd)$_2$–$Bi(C_6H_5)_3$–$Ta(OC_2H_5)_5$ [104] systems. On the other hand, despite the vaporization and stability advantages, the use of fluorine containing precursors for SBT deposition has been hampered by fluorine incorporation in as-deposited films (see previous section) that seems not to be compatible with good electrical properties. The Sr(hfac)$_2$tetraglyme precursor has been, however, successfully used for fabrication of ferroelectric SBT adopting plasma-enhanced MOCVD [105], as well as classical MOCVD reactors [89,106,107]. These studies showed that the multi-component process adopting the Sr(hfac)$_2$tetraglyme, $Ta(OC_2H_5)_5$ and $Bi(C_6H_5)_3$ precursor system involves complex deposition kinetics. The processes of individual Sr(hfac)$_2$tetraglyme, $Bi(C_6H_5)_3$ and $Ta(OC_2H_5)_5$ sources have been addressed in detail in several papers [72,75,106,108]. Thus, depositions from Sr(hfac)$_2$tetraglyme and $Bi(C_6H_5)_3$ lead to formation of polycrystalline SrF_2 and Bi_2O_3, respectively. By contrast, films deposited from $Ta(OC_2H_5)_5$ are amorphous TaO_x oxides. XPS depth profiles have shown that in all cases there is no significant carbon contamination.

Deposition of SBT adopting the combined Sr(hfac)$_2$tetraglyme, $Bi(C_6H_5)_3$ and $Ta(OC_2H_5)_5$ sources has been usefully compared to processes associated with each singular precursor [89,106,107]. The logarithmic plots of growth rates of SrF_2, Bi_2O_3 and TaO_x versus reciprocal temperature (Fig. 13) for the multi-component process are compared with similar plots for single component processes.

Trends observed in both single and multi-component processes, clearly indicate that deposition temperatures in the 450–500 °C range are the most suited for the deposition of Sr–Bi–Ta–O(F) matrices with the correct stoichiometry. In this temperature range the Sr, Bi and Ta growth rates are comparable

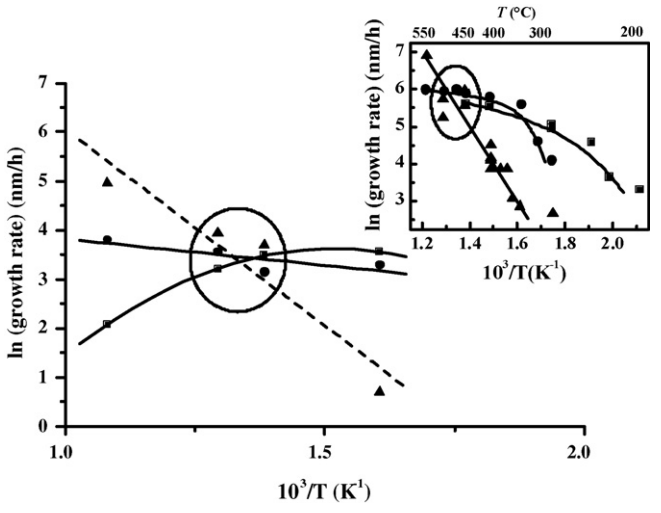

Fig. 13. Logarithmic plots of growth rates of SrF_2, Bi_2O_3 and TaO_x vs. reciprocal deposition temperature during the multi-component process. Inset shows similar plots for single component processes: (●) Sr; (▲) Bi; (■) Ta [107].

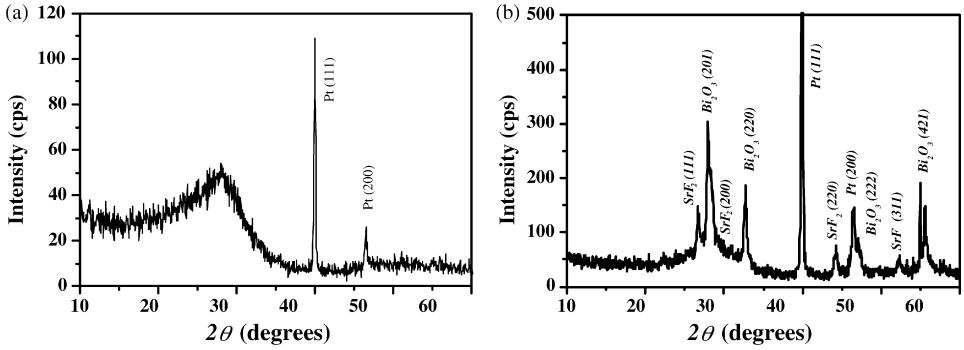

Fig. 14. Typical XRD patterns in grazing incidence of films deposited on Pt at (a) 450 °C and (b) 500 °C [107].

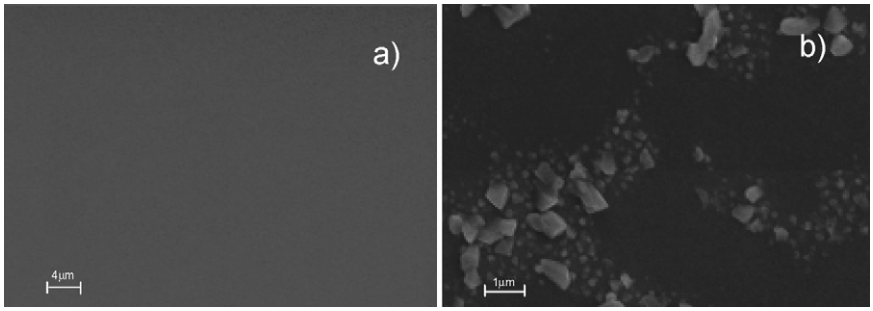

Fig. 15. Typical SEM micrographs of films deposited on Pt at (a) 450 °C and (b) 500 °C [107].

and, even more important, Sr and Ta rates can be easily controlled since both are almost insensitive to the deposition temperature. The control of the Bi concentration remains, however, much more critical since the related deposition rate depends on the temperature. GIXRD patterns and SEM micrographs provide evidence that films deposited at 450 °C (Figs. 14a and 15a) are homogenous and amorphous while films deposited at 500 °C (Fig. 14b) consist of polycrystalline SrF_2 and Bi_2O_3 and amorphous TaO_x. The latter films are not homogeneous since Bi-excess grains of about 200–300 nm are present (Fig. 15b). In all cases films do not show evidence of carbon contamination.

Post-deposition O_2 annealing of Sr–Bi–Ta–O(F) matrix in the 650–700 °C range causes the formation of both SBT and of a non-stoichiometric fluorite phase [109,110]. By contrast, annealing at 800 °C forms randomly oriented polycrystalline SBT films without cracks (Fig. 16).

AFM images (Fig. 17) of (a) as-deposited films at 450 °C (roughness $\sim 4 \pm 1$ nm) and (b) films annealed at 800 °C (roughness $\sim 13 \pm 1$ nm), show, in both cases, 250–350 nm size grains with an overall thickness around 160 nm.

It is worthy of note that the thermal treatment (800 °C) has proved suitable for the complete elimination of any fluorine-containing phases [107]. The related *P–E* hysteresis loop (Fig. 18) indicates the ferroelectric character of the SBT film with remnant ($2P_r = 18.7\ \mu C\ cm^{-2}$) and saturation polarizations ($2P_{sat} = 50\ \mu C\ cm^{-2}$ at 500 kV/cm) totally comparable with typical values of SBT thin films obtained either by MOD [111,112] or by liquid-delivery MOCVD of fluorine-free precursors [113]. Therefore, electrical data agree well with the ferroelectric response of a pure SBT phase without any fluorine contaminant and non-stoichiometric fluorite phase.

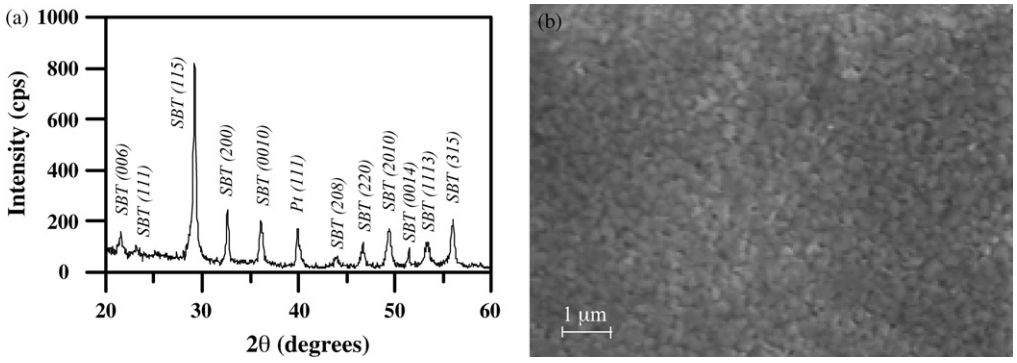

Fig. 16. Typical (a) GIXRD pattern and (b) SEM micrograph of SBT films deposited on Pt at 450 °C and annealed at 800 °C under O_2 flow [107].

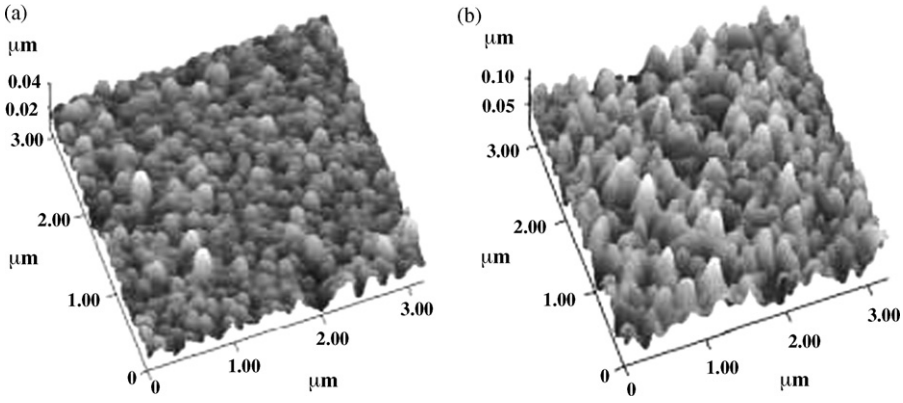

Fig. 17. AFM images of films (thickness 160 nm) deposited on Pt (a) at 450 °C and, then, (b) annealed at 800 °C under O_2 flow [107].

2.6. Fabrication of double sided TlBaCaCuO superconducting films from fluorine containing multi-element source

Microwave passive devices for telecommunications such as resonators, filters and antennae are some of the main applications of high critical temperature (T_c) superconducting materials [114–116]. In particular, the perovskite mixed oxide TlBaCaCuO system is particularly interesting due to the high T_c values of various Tl based phases. Fabrication of double sided (DS) $Tl_2Ba_2CaCu_2O_8$ (Tl-2212) films on $LaAlO_3$ (1 0 0) [117], a substrate with a low microwave loss, represents a case study of applications of the Ba(hfac)$_2$tetraglyme and Ca(hfac)$_2$tetraglyme precursors. In this case the feasibility of the process has been largely associated with the peculiar properties of the multimetal single-source used for the preliminary MOCVD fabrication of BaCaCuOF matrices. This novel approach, based on a single-source multimetal mixture in a monocomponent hot-wall reactor, has been found ideally suited for a uniform coating of both sides of the $LaAlO_3$ (1 0 0) substrate. The multicomponent precursor consists of a homogeneous mixture of Ba(hfac)$_2$tetraglyme, Ca(hfac)$_2$tetraglyme and Cu(tmhd)$_2$ in an appropriate stoichiometric ratio.

The adopted protocol represents a general purpose route for fabrication of materials containing a large variety of metal elements using a multi-component single source.

The differential scanning calorimetry (DSC) analysis of a 3.0:1.0:0.5 multi-component (Ba, Ca and Cu) source, compared with those of each individual precursor is reported in Fig. 19. The DSC scan of the multi-component mixture shows a single sharp endothermic peak at 89.9 °C, which may be associated with melting of the Ca(hfac)$_2$tetraglyme component, while the sharp peaks observed in the curves of the Ba and Cu single precursors, corresponding to the melting of the Ba(hfac)$_2$tetraglyme (153.6 °C) and Cu(tmhd)$_2$) (196.3 °C) complexes are not present. These data indicate that the Ca(hfac)$_2$tetraglyme acts, upon melting, as a solvent for the other companion sources (Ba and Cu) thus giving rise to a homogenous multimetal liquid single source. Nevertheless, it can not be excluded the possibility that the peak at 89.9 °C, which is slightly lower than the melting point reported for Ca(hfac)$_2$tetraglyme, is the melting of a binary or ternary eutectic mixture. The endothermic broad peak observed in the DSC curve of the mixture in the 110–160 °C temperature range is likely associated with Ba(hfac)$_2$tetraglyme and Cu(tmhd)$_2$ dissolution. The highest temperature (190–270 °C) endothermic process is associated with evaporation of the melt mixture.

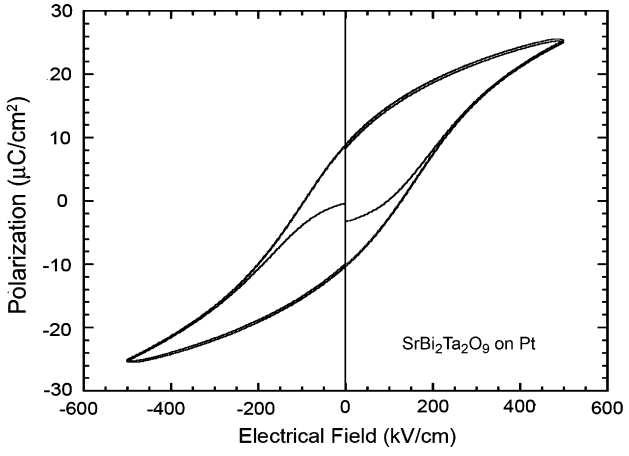

Fig. 18. Hysteresis loop measured on a SBT film (thickness 110 nm) deposited on Pt at 450 °C then annealed at 800 °C under O_2 flow [107].

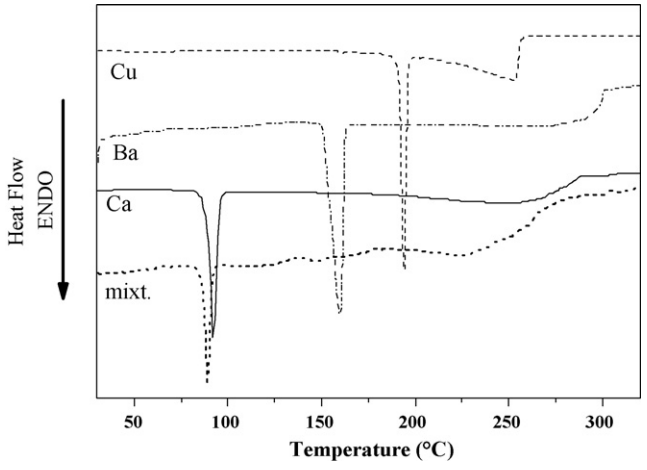

Fig. 19. DSC curve of the Ba–Ca–Cu mixture compared with data of individual precursors, Ba(hfac)$_2$tetraglyme, Ca(hfac)$_2$tetraglyme, Cu(tmhd)$_2$ [117].

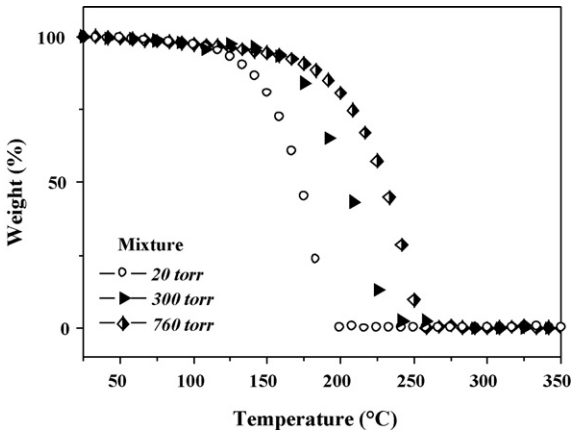

Fig. 20. TG profiles of the Ba–Ca–Cu mixture under N_2 flow in the 25–350 °C temperature range at 20, 300 and 760 Torr (heating rate 5 °C/min)[118].

Optical polarized light microscopy observations upon heating confirm these conclusions.

TG measurements carried out at 20, 300 and 760 Torr indicate that the multi-component Ba–Ca–Cu source vaporizes in a single step, not dependent on the pressure (Fig. 20) [118]. Nevertheless, a significant decrease of vaporization temperature is observed under reduced pressure (20 Torr), i.e. under experimental conditions closely comparable to those used in the MOCVD process.

Low pressure (20 Torr) isothermal thermogravimetric analysis (ITG) of the molten Ba–Ca–Cu single source in the 100–150 °C temperature range under N_2 (Fig. 21a) points to an almost linear behavior with vaporization time. In particular, a linear dependence is observed in the 100–120 °C temperature range. This is indication of no secondary phenomena that could affect mass transport (such as decomposition or polymerization). At the highest temperature (150 °C) a non-linear behavior is observed thus suggesting that contributions of individual precursors prevail giving rise to differential vaporization rates.

Similarly, the Arrhenius plot of the same multi-component source (Fig. 21b) shows in the 100–120 °C range, a linear trend totally analogous to those of efficient, thermally stable single precursors.

The DS Tl based films on $LaA1O_3$ (1 0 0) exhibit XRD patterns (Fig. 22) indicative of well-crystallised *c*-axis oriented Tl-2212 phase. The (1 0 7) pole figure of a 5 μm thick DS-Tl-2212 film (inset in Fig. 22) indicates an epitaxial high quality Tl-2212 phase. SEM micrographs of both sides (Fig. 22) show dense and homogeneous structures consisting of smooth overlapping platelets roughly up to 10 μm diameter.

The transport properties of Tl films, key diagnostics to film quality and applications readiness, show good J_c and T_c values [$J_{c,1}$ (77 K) = 3×10^4 A/cm^2, $T_{c,1}$ = 98.5 K and $J_{c,2}$ (77 K) = 7×10^4 A/cm^2, $T_{c,2}$ = 100 K, with $\Delta T_c = 1$ in both cases] (Fig. 23). Surface resistance data similarly indicate that these films are very promising for passive filter applications.

To conclude, this class of novel, molecularly engineered precursors represents a challenging application of a multimetal single source. It offers the best promise for a scalable and reproducible deposition technology due to the overall simplification of the MOCVD process in terms of both reproducibility and accurate control of matrix stoichiometry.

3. Engineering of rare earth precursors for multi-source MOCVD of functional oxides

3.1. MOCVD processes from fluorinated and fluorine-free La precursors

In the wide scenario of emerging materials, rare earth elements are components of several interesting new materials with properties ranging from high T_c superconductors, such as $LnBa_2Cu_3O_{7-\delta}$ [119,120], $Pb_2Sr_2LnCu_3O_{8-\delta}$ [121] and $La_{2-x}Sr_xCuO_4$ [122] to piezoelectrics such as $LaCuO_2$ [123]; from buffer layers such as $LaAlO_3$ [56,124,125], $YAlO_3$ [126] and CeO_2 [127,128] to high *k* dielectrics such as Pr_2O_3 [129]. Lanthanum oxide is also a key material for the development of ferroelectric material. In particular, La-doped $Bi_4Ti_3O_{12}$ (BLT) and La-doped $(Pb_xZr_{1-x})TiO_3$ represent new materials for non-volatile ferroelectric memories [130–135]. Finally, $(La_xA_{1-x})MnO_3$ (A = Sr, Ca, Ba, etc.) oxides show colossal magnetoresistance properties (CMR) [136–138]. These materials all require suitable fabrication methodologies in the form of thin films that represent an unavoidable demand for their functional applications in emerging technologies. MOCVD is

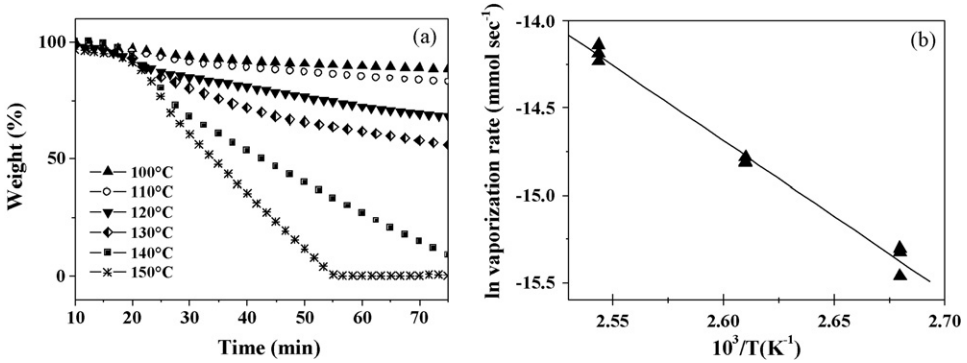

Fig. 21. (a) Isothermal mass (%) vs. time of vaporization of the Ba–Ca–Cu mixture under N_2 flow in the 100–150 °C temperature range at 20 Torr and (b) Arrhenius plot derived from mass-loss data [118].

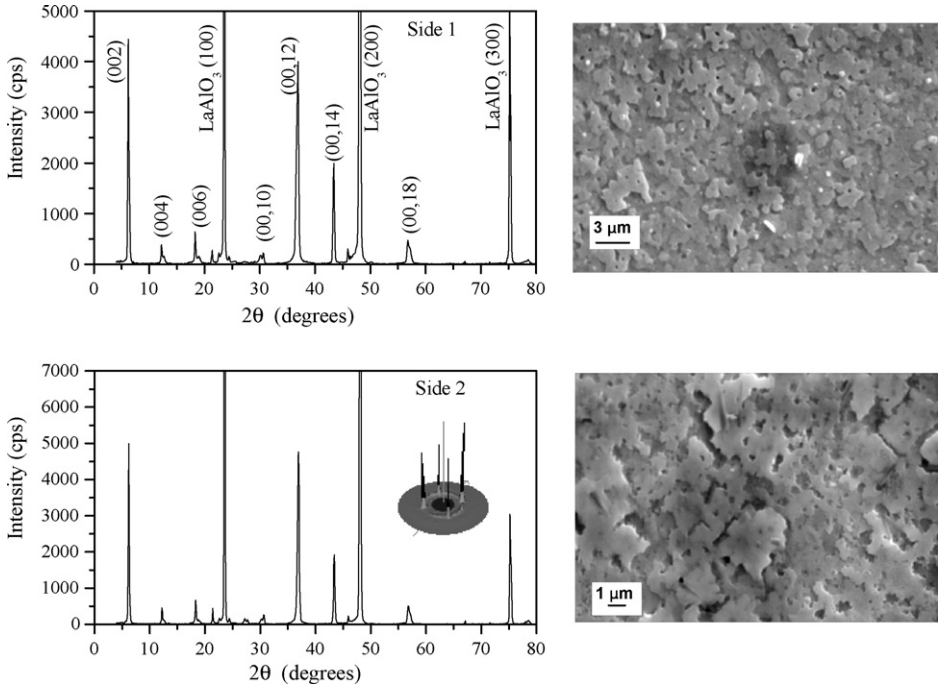

Fig. 22. Left side: XRD patterns of a DS Tl-2212 film grown on $LaAlO_3$ (1 0 0) substrate. The inset shows the (1 0 7) pole figure of one side of the DS $Tl_2Ba_2CaCu_2O_8$ film. Right side: SEM images of the DS Tl-2212 film grown on $LaAlO_3$ (1 0 0) substrate [117].

now well recognized as a primary road to this manufacture [99–101]. Ideally, suitable precursors are also required not only in terms of good volatility and thermal stability but also in terms of decomposition processes suited to deposit good quality films. Similarly to group II metals, the conventional, "first generation", rare earth β-diketonate precursors have shown low vaporization rates and poor stability to the atmosphere, whilst second-generation rare-earth precursors combining fluorinated β-diketonates and polyethers show improved thermal stabilities and volatilities compared to classical non-fluorinated La(β-diketonate)$_3$. Fluorinated precursors were proved well suited for the synthesis of fluoride and oxyfluoride phases as well as for the synthesis of multi-component lanthanide containing oxides. In the case of electroceramic oxides, fluorinated precursors might, however, have some drawbacks due to the possible incorporation of fluorine contaminants which are highly undesired. Worthy of note in this context that fluorine-free "first generation" precursors, although less volatile and thermally stable than fluorinated β-diketonate polyether adducts, have been widely applied to deposition of lanthanide oxides adopting both classical and DLI equipped reactors [139–142]. Nonetheless, La_2O_3 films grown from classical La(tmhd)$_3$ and La(acac)$_3$ (acac = acetylacetonate) sources bear heavy carbon contamination for reasons which are not yet completely understood [139–143] even though similarities with group II metal β-diketonate seem evident. Some papers have reported that carbon free La-containing phases can be also obtained from fluorine-free precursors adopting either ALD processes [141] or slow growth rate MOCVD processes [144]. Thus in the latter case, films deposited using La(tmhd)$_3$ and La(tmod)$_3$ consist (Fig. 24a) of different phases, namely La_2O_3 contaminated with noticeable amounts of other phases associated with the poor chemical stability in air of La_2O_3 that transforms to monoclinic LaO(OH), La(OH)$_3$ and to lanthanum oxide carbonate $La_2O_2CO_3$ [141,142,145–147]. In fact, LaO(OH) is clearly evident in diffuse reflectance absorption FT-IR (DRIFT) spectrum (Fig. 24b). It shows a strong band at 3450 cm^{-1} and a doublet at 765 and 700 cm^{-1} associated with hydroxyl group vibrations. [142,147] Moreover, the doublet at 470 and 515 cm^{-1} represents the La–O stretching associated with La_2O_3 and LaO(OH), respectively.

XPS in-depth profiles (Fig. 25) of the same films indicate that the carbonate is a surface phase while no carbon contamination is present in the bulk. In fact, the C 1s feature disappears after a few minutes of Ar^+-ion etching as expected for contaminants purely due to air exposure and not to by-products accompanying the precursor decomposition (such as CO_2).

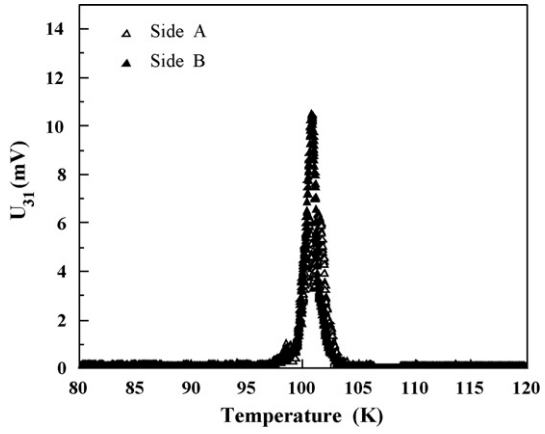

Fig. 23. T_c inductive measurements of a typical DS $Tl_2Ba_2CaCu_2O_8$ film [117].

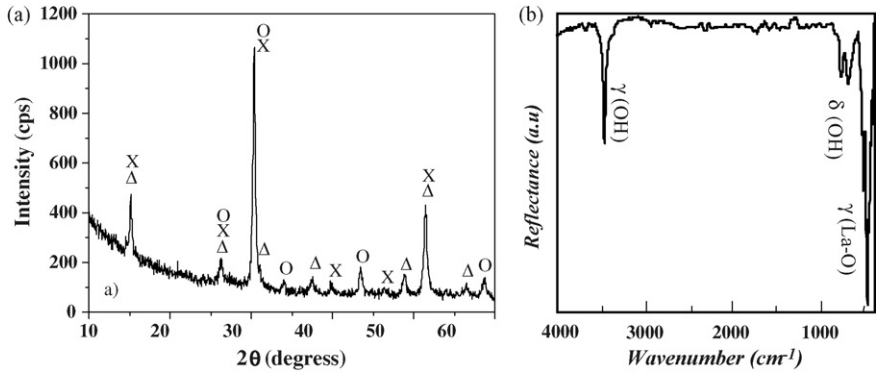

Fig. 24. Typical XRD pattern (a) and DRIFT spectrum (b) of samples deposited on Pt at 450 °C: (◯) hexagonal La_2O_3 phase; (×) hexagonal $La_2O_2CO_3$phase; (△) monoclinic LaO(OH) phase [144].

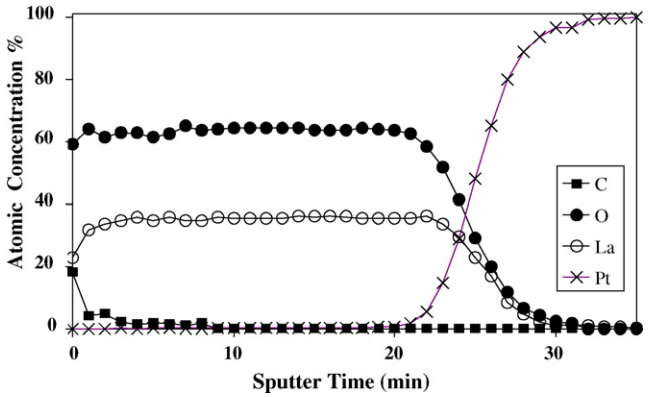

Fig. 25. XPS in-depth profile of a La-containing film deposited at 450 °C from fluorine-free precursors [144].

Note that the relatively slow growth rate (30–100 nm/h) compared to usual values (250–1000 nm/h) seems to be a key issue to preclude carbonate contamination since CO_2 formation remains marginal under these conditions.

By contrast, typical MOCVD experiments adopting La(hfac)$_3$diglyme yield films consisting of the hexagonal LaF_3 phase (Fig. 26) from 300 °C up to about 600 °C independent of the oxygen flow [148]. The unusually intense (0 0 2) peak, compared to the 100% intensity value expected for the (1 1 1) reflection in polycrystalline films, is a clear indication of [0 0 1] texturing.

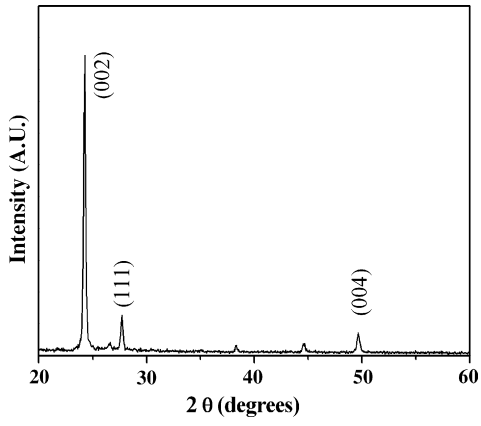

Fig. 26. θ–2θ XRD pattern of a lanthanum containing film deposited at 550 °C [148].

3.2. *Decomposition pathways of second generation La(hfac)$_3$diglyme compared to classical La(tmhd)$_3$ and La(tmod)$_3$ sources in MOCVD processes*

Information on decomposition pathways of fluorine-free precursors compared to fluorinated ones has been obtained by the real-time monitoring of the nature and composition of the gas-phase in MOCVD/FT-IR experiments.

Thus, IR absorbance values (namely, the C–H stretching (νCH) at 2970 cm^{-1} and the C=O stretching (νCO) at 1550 cm^{-1}) of gas phase La(tmhd)$_3$ decrease monotonically, above 200 °C (Fig. 27). Above 300 °C, the νCO band broadens and a shoulder appears at 1606 cm^{-1}. These features can be associated with the free tmhd ligand. Above 450 °C, νCO and νCH bands disappear completely and two new IR modes at 1730 cm^{-1}, associated with ketone by-products, and at 2295 cm^{-1}, associated with CO_2, become evident [69,84–87].

Similar trends (Fig. 28) are obtained with La(tmod)$_3$. Nevertheless in this case, decomposition of the hydrocarbon moiety (νCH) is less evident than the ring decomposition (νCO). A new band at 1730 cm^{-1} due to ketone by-products becomes apparent above 200 °C and steadily increases with the temperature. Above 300 °C, the feature at 1604 cm^{-1} associated with the free tmod ligand, becomes apparent. Above 450 °C, there is evidence of total demolition of precursor with formation of CO_2. Therefore, both La(tmhd)$_3$ and La(tmod)$_3$ precursors decompose at low temperature ($T > 200$ °C). Decomposition, however, of La(tmod)$_3$ involves the breakdown of the β-diketonate ring with the formation of ketones and free Htmhd which both leave CH_3 methyl groups intact. By contrast, La(tmhd)$_3$ decomposes involving the oxidation of both the β-diketonate ring and the CH_3 moiety probably on the reactor walls leading to oxidation by-products. Only above 450 °C does the decomposition of the two precursors become similar since it leads in both cases to the demolition of both ring and hydrocarbon moieties with the formation of CO_2 and ketone by-products.

FT-IR/MOCVD experiments of the fluorinated La(hfac)$_3$diglyme source suggest different decomposition pathways (Scheme 5). Gas phase spectra do not show signif-

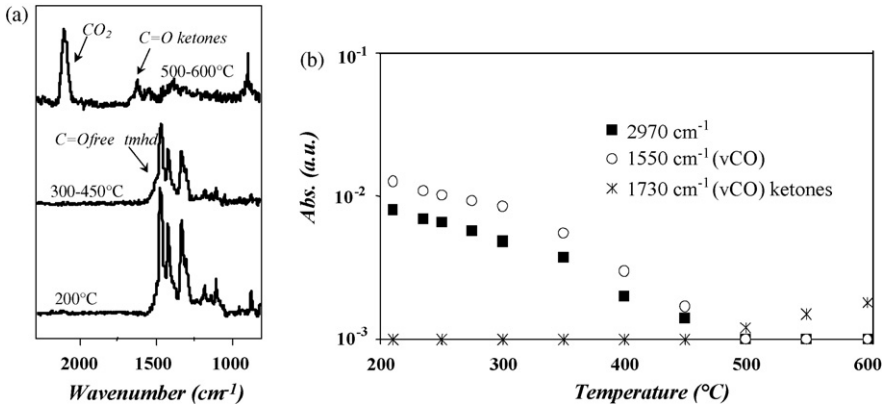

Fig. 27. (a) *In situ* FT-IR spectra of La(tmhd)$_3$ at several temperatures: 200 °C, 300–450 °C and 500–600 °C. (b) Dependence of the absorbance of the main IR bands upon temperature during MOCVD under Ar/O_2 [144].

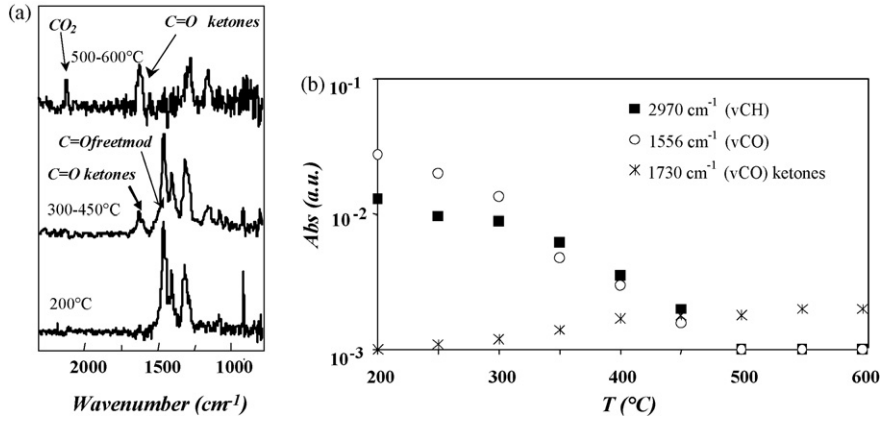

Fig. 28. (a) *In situ* FT-IR spectra of La(tmod)$_3$ at several temperatures 200 °C, 300–450 °C and 500–600 °C and (b) dependence of the absorbance of the main IR bands on temperature during MOCVD under Ar/O_2 [144].

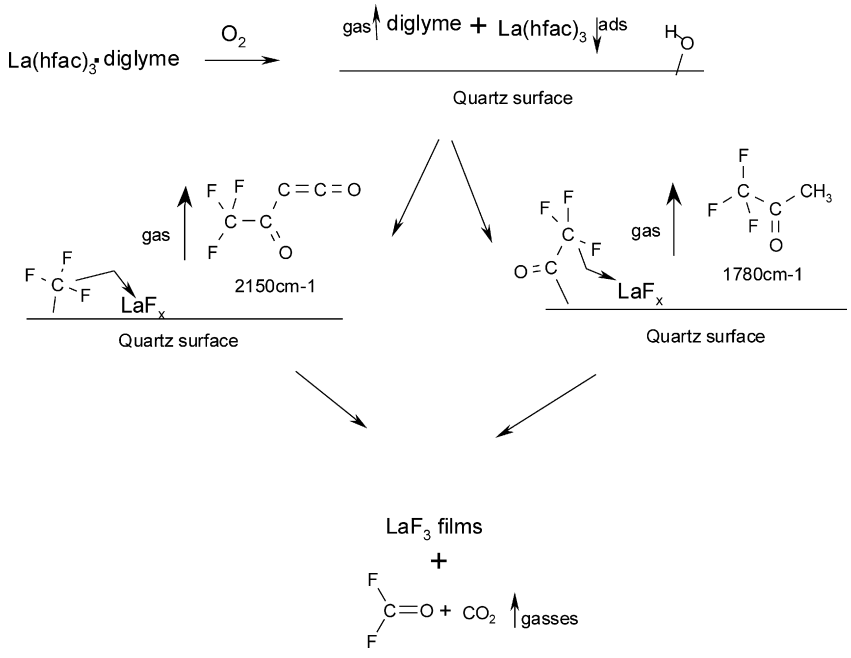

Scheme 5.

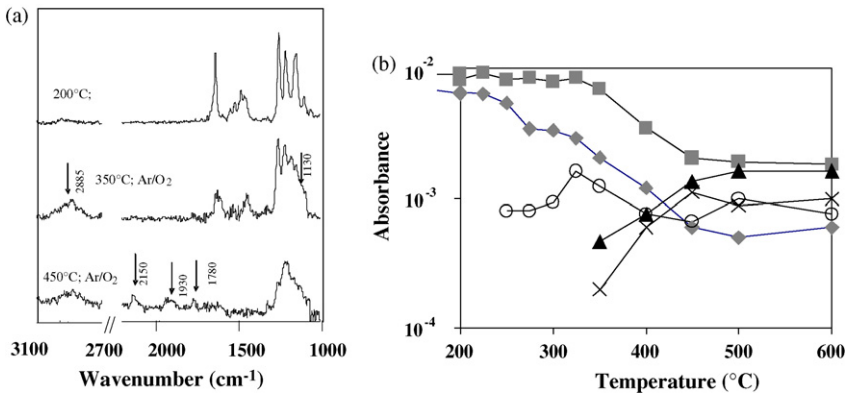

Fig. 29. (a) *In situ* IR spectra of La(hfac)$_3$diglyme at various reactor temperatures in the 200–550 °C range. (b) Dependences of the absorbances of important IR bands vs. T°C: (■) 1255 cm^{-1} (La(hfac)$_3$diglyme, C–F stretch); (♦) 1650 cm^{-1} (La(hfac)$_3$diglyme, C=O stretch); (▲) 1780 cm^{-1} (C=O stretch, fluorinated ketones); (×) 2150 cm^{-1} (C=C=O stretch, acylketenes); (◯) 2885 cm^{-1} (C–H stretches, diglyme). All experiments were carried out under Ar/O_2 [67].

icant changes of the relevant spectral features up to 350 °C (Fig. 29a). Above this temperature, the presence of O_2 admixture in the stream favors the polyether dissociation and IR spectra at 350 °C show the characteristic bands of the free ancillary glyme ligand (2885 and 1130 cm^{-1}). The temperature dependence of the dissociative pathway is shown in Fig. 29b. The C–H_x stretches of unbounded diglyme are apparent even at 250 °C and their intensities increase above this temperature. A maximum value is observed at 350 °C. Above this temperature much more complex processes occur and other reaction products are observed. In particular the IR features at 2150 cm^{-1}, 1780 cm^{-1} and around 1930 cm^{-1} can be associated with ketenes, fluorinated ketones and oxidized compounds (such as CF_2CO), respectively.

3.3. A case study: the in situ synthesis of superconducting $La_{2-x}Ba_xCuO_{4+\delta}$ thin film

The $La_{2-x}Ba_xCuO_{4+\delta}$ (LBCO) phase is the first high temperature superconducting cuprate discovered in 1986. Even though the La(Ba)–Cu–O phase has great possibility to achieve critical temperature (T_c) values as high as 44 K, there are relatively few reports about the preparation of related thin films. In fact, the almost coincident discovery of new superconductors with even higher T_c values such as YBaCuO, BiSrCaCuO, TlBaCaCuO, has attracted more attention and these have overshadowed interest in the LBCO phase.

The MOCVD *in situ* fabrication of superconducting $La_{2-x}Ba_xCuO_{4+\delta}$ (LBCO) films represents a case application of both a rare-earth and an alkaline-earth metal precursor. Again, the multi-element single source, consisting of a suited mixture of La(hfac)$_3$diglyme, Ba(hfac)$_2$tetraglyme, and Cu(tmhd)$_2$ in an appropriate stoichiometric ratio, has been expedient for the process [58]. The molten La adduct behaves as a solvent for both the Ba and Cu sources, thus forming a real multi-element single-source.

The linear trend of the Arrhenius plot related to isothermal mass loss in the 90–110 °C interval (Fig. 30) indicates no side decomposition thus showing thermal and mass transport properties suited for MOCVD processes.

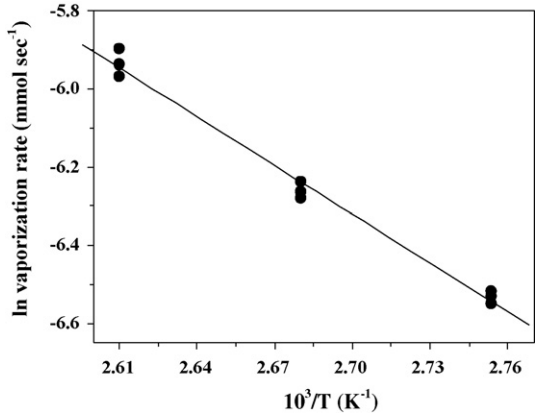

Fig. 30. Arrhenius plot for the vaporization of the La–Ba–Cu mixture in the 1.8:1.0:0.1 ratio under N_2 flow at 20 Torr [58].

Best quality films in terms of structural data and composition form upon evaporation at 90 °C from the molten mixture and deposition at 800 °C. The XRD of a typical *in situ* grown $La_{2-x}Ba_xCuO_{4+\delta}$ film is shown in Fig. 31. In these conditions, monophasic *c*-axis oriented LBCO films are formed since only the (0 0 *l*) reflections are present. In addition, the four maxima

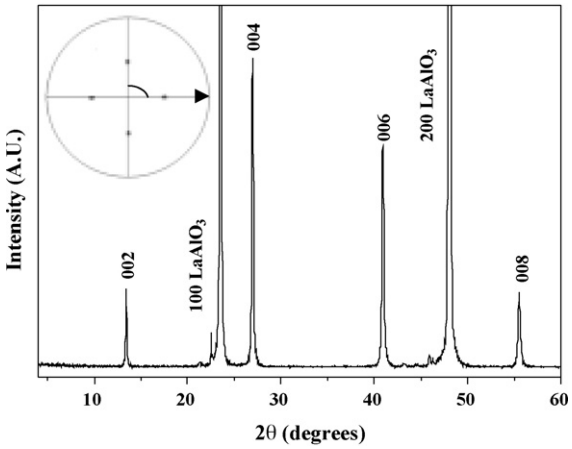

Fig. 31. XRD pattern of a *c*-axis oriented $La_{2-x}Ba_xCuO_{4+\delta}$ film grown on $LaAlO_3$ (1 0 0). The inset shows the (1 0 3) pole figure [58].

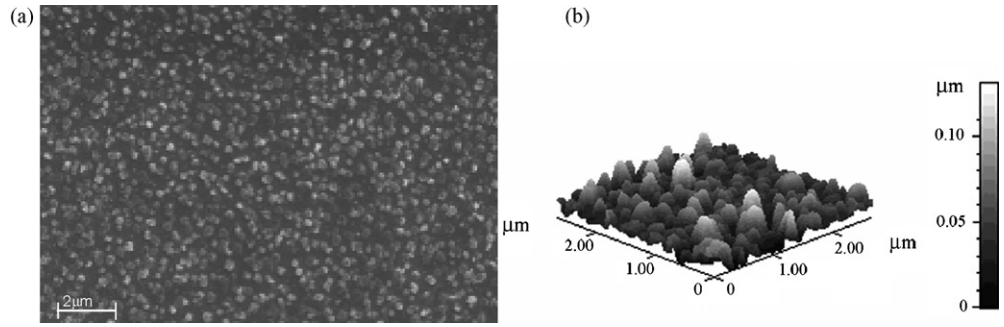

Fig. 32. SEM (a) and AFM (b) images of a *c*-axis oriented $La_{2-x}Ba_xCuO_{4+\delta}$ film grown on $LaAlO_3$ (1 0 0) [58].

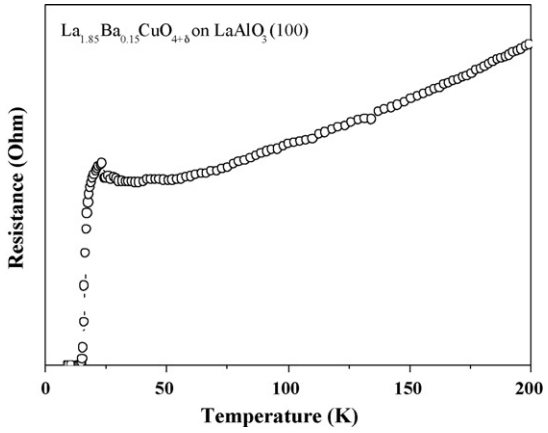

Fig. 33. Variable-temperature resistance data of an *in situ* grown $La_{1.85}Ba_{0.15}CuO_{4+\delta}$ film [58].

observed at $\Psi = 49^\circ$ of the (1 0 3) pole figure (inset in Fig. 31) clearly point to epitaxial growth of LBCO film on $LaAlO_3$ (1 0 0) substrates.

Surface morphology of LBCO samples (Fig. 32) deposited on $LaAlO_3$ substrates consists of a fine-grained structure with grains of about 400 nm. The surface roughness of films has been investigated using AFM (Fig. 32b). The root mean square (RMS) roughness of the film surface measured on a 2.5 μm × 2.5 μm area was 20.2 nm.

Typical resistive measurements performed as a function of temperature, reported in Fig. 33, indicate that the resistivity of these films is metallic ($d\rho/dT > 0$) with an onset of the transition temperature $T_c = 27$ K.

4. Conclusions

The present review has focused on the relationship between precursor nature and materials properties through a detailed study of the precursor thermal properties and the decomposition mechanism as well as deposition kinetics. Various precursors of large ionic radius of both alkaline-and rare-earth metals have been considered. This study represents a comprehensive view of characteristics and properties of both fluorine-free and fluorinated precursors considering advantages and drawbacks in relation to MOCVD applications.

In regard to alkaline-earth metals, the comparison between MOCVD processes adopting the $Sr(tmhd)_2$pmdeta and $Sr(hfac)_2$tetraglyme precursors indicates that the non-fluorinated precursor causes the formation of ketones and other oxidation products (such as CO_2) and leads to $SrO/SrCO_3$ films, while the $Sr(hfac)_2$tetraglyme produces fluorinated molecules (CF_2O and ketenes) and this ligand fragmentation leads to the formation of SrF_2 films. Therefore both precursors require annealing treatments to eliminate carbonate or fluoride phases from deposited films. In this context it is important to note that the disadvantage of the use of a fluorinated precursor (due to the severe annealing conditions often required for fluorine elimination) can be partially counterbalanced by the better transport properties of the $Sr(hfac)_2$tetraglyme. In addition, we note that application of the $Sr(hfac)_2$tetraglyme precursor to fabrication of a multielement system such as SBT has produced fluorine-free films without the need of a hydrolysis step. In fact, XRD data indicate a pure polycrystalline SBT phase without any remaining fluorite phase. Applications of homologous precursors of Ba and Ca have produced good quality fluorine free double sided TlBaCaCuO films. Also in this case no hydrolysis step is needed to eliminate fluorine from the BaCaCuO(F) matrices since the fluoride phases react with Tl(I) oxide and produce pure superconducting TlBaCaCuO films.

Analogously, the $La(hfac)_3$diglyme precursor has proved to be stable during both the sublimation and transport processes from the supply reservoir to the reactor. The FT-IR study has demonstrated the important role of diglyme which appeared to be strongly bonded to the metal thus providing the stability required for sublimation and mass transport. On the other hand, the presence of O_2 during the film deposition process has been proved effective in promoting diglyme dissociation and, hence, in preventing the carbon contamination in the LaF_3 films. Similarly to the $Sr(hfac)_2$tetraglyme, CF_2O, ketenes and fluorinated ketones are the main decomposition products of the $La(hfac)_3$diglyme, while CO_2 and ketones are typical by-products of classical $La(tmhd)_3$ and $La(tmod)_3$ precursors. Although these classical non-fluorinated precursors possess lower thermal stability and vaporization rates compared to hexafluoroacetylacetonate adducts [55] they are also suitable DLI-MOCVD sources since carbon-free films can be obtained in slow rate MOCVD processes [144].

In regard to the application of fluorinated precursors to a complex oxide system, good quality epitaxial LBCO films have been grown through an *in situ* MOCVD process. The approach used, which takes advantage of a simple multi-metal single

source consisting of an intimate mixture of $Ba(hfac)_2$tetraglyme, $Cu(tmhd)_2$ and $La(hfac)_3$diglyme in an optimized ratio, can easily control the stoichiometry of deposited films.

Finally, it is worth noting that examples reported in this review demonstrate that fluorine-containing precursors may be used to fabricate fluorine-free multielement systems. In fact, present data have demonstrated that pure advanced materials such as ferroelectric SBT, superconducting TlBaCaCuO and La(Ba)CuO films can be grown with simple MOCVD processes adopting $M(hfac)_n$glyme precursors, which are very stable for storage and manipulation. Thus, the problem of unwanted fluorinated phases should be addressed each time, depending on the metallic nature and thermodynamic stability of the desired phase.

One of the future challenges in the field of precursors for fabrication of advanced materials regard the syntheses of heteronuclear complexes. The aim of these syntheses is to tailor the molecular structure of the single source MOCVD precursor in order to have a metal ratio in the source fitting the stoichiometry of the final product.

Acknowledgements

The authors wish to thank the MIUR for the financial support within the FISR thematic activities "Nanosystems of transition metal oxide for solid oxide fuel cells (SOFCs) (New systems for energy production and storage program)"; PRIN 2005 "Auto-organizzazione di architetture molecolari su superfici inorganiche" and FIRB 2003 "Composti molecolari e materiali ibridi nanostrutturati con proprietà ottiche risonanti e non-risonanti per dispositivi fotonici" projects.

References

[1] J.G. Bednorz, K.A. Mueller, Z. Phys. B 64 (1986) 189.
[2] M.K. Wu, J.R. Ashburn, C.J. Torng, P.H. Hor, R.L. Meng, L. Gao, Z.J. Huang, Y.Q. Wang, C.W. Chu, Phys. Rev. Lett. 58 (1987) 908.
[3] H. Maeda, Y. Tanaka, M. Fukutomi, T. Asano, Jpn. J. Appl. Phys. Part 2 27 (1988) L209.
[4] Z.Z. Sheng, A.M. Hermann, Nature 332 (1988) 55;
Z.Z. Sheng, A.M. Hermann, Nature 332 (1988) 138.
[5] M.L. Hitchman, K.F. Jensen, Chemical Vapor Deposition: Principles and Applications, Academic Press, London, 1993.
[6] R.C. Mehrotra, R. Bohra, D.P. Gaur, Metal β-Diketonates and Allied Derivatives, Academic Press, London, 1978.
[7] M. Leskelä, H. Mölsä, L. Niinistö, Supercond. Sci. Technol. 6 (1993) 627, and refs. therein.
[8] T. Nakamura, K. Tachibana, Jpn. J. Appl. Phys. Part 1 40 (2001) 338.
[9] M. Yamamuka, S. Momose, T. Nakamura, K. Tachibana, H. Takada, Jpn. J. Appl. Phys. Part 1 41 (2002) 2231.
[10] S. Momose, T. Nakamura, K. Tachibana, Jpn. J. Appl. Phys. Part 1 39 (2000) 5384.
[11] T. Kimura, H. Yamauchi, H. Machida, H. Kokubun, M. Yamada, Jpn. J. Appl. Phys. Part 1 33 (1994) 5119.
[12] C.A.-P. de Araujo, J.D. Cuchiaro, L.D. McMillan, M.C. Scott, J.F. Scott, Nature 374 (1995) 627.
[13] F. Weiss, J. Lindner, J.P. Senateur, C. Dubourdieu, V. Galindo, M. Audier, A. Abrutis, M. Rosina, K. Frohlich, W. Haessler, S. Oswald, A. Figueras, J. Santiso, Surf. Coat. Technol. 133/134 (2000) 191.
[14] R. Gardiner, D.W. Brown, P.S. Kirlin, A.L. Rheingold, Chem. Mater. 3 (1991) 1053.
[15] J. Brooks, H.O. Davies, T.J. Leedham, A.C. Jones, A. Steiner, Chem. Vap. Depos. 6 (2000) 66.
[16] A.D. Berry, R.T. Holm, M. Fatemi, D.K. Gaskill, J. Mater. Res. 5 (1990) 1169.
[17] A.C. Jones, J. Mater. Chem. 12 (2002) 2576.
[18] S.R. Drake, A. Lyons, D.J. Otway, A.M.Z. Slawin, D.J. Williams, J. Chem. Soc., Dalton Trans. 19 (1993) 2379.
[19] G. Xu, Z.-M. Wang, Z. He, Z. Lüe, C.-S. Liao, C.-H. Yan, Inorg. Chem. 41 (2002) 6802.
[20] K. Timmer, K.I.M.A. Spee, A. Mackor, H.A. Meinema, A.L. Spek, P. van der Sluis, Inorg. Chim. Acta 190 (1991) 109.
[21] K. Timmer, H.A. Meinema, Inorg. Chim. Acta 187 (1991) 99.
[22] P. van der Sluis, A.L. Spek, K. Timmer, H.A. Meinema, Acta Crystallogr. C 46 (1990) 1741.
[23] S.R. Drake, S.A.S. Miller, D.J. Williams, Inorg. Chem. 32 (1993) 3227.
[24] J.A.T. Norman, G.P. Pez, J. Chem. Soc., Chem. Commun. (1991) 971.
[25] S.C. Thompson, D.J. Cole-Hamilton, D.D. Gilliland, M.L. Hitchman, J.C. Barnes, Adv. Mater. Opt. Electron. 1 (1992) 81.
[26] G. Malandrino, F. Castelli, I.L. Fragalà, Inorg. Chim. Acta 224 (1994) 203.
[27] G. Malandrino, I.L. Fragalà, D.A. Neumayer, C.L. Stern, B.J. Hinds, T.J. Marks, J. Mater. Chem. 4 (1994) 1061.
[28] D.A. Neumayer, D.B. Studebaker, B.J. Hinds, C.L. Stern, T.J. Marks, Chem. Mater. 6 (1994) 878.
[29] J.A.P. Nash, J.C. Barnes, D.J. Cole-Hamilton, B.C. Richards, S.L. Cook, M.L. Hitchman, Adv. Mater. Opt. Electron. 5 (1995) 1.
[30] J.A. Belot, D.A. Neumayer, C.J. Reedy, D.B. Studebaker, B.J. Hinds, C.L. Stern, T.J. Marks, Chem. Mater. 9 (1997) 1638.
[31] G. Malandrino, D.S. Richeson, T.J. Marks, D.C. DeGroot, J.L. Schindler, C.R. Kannewurf, Appl. Phys. Lett. 58 (1991) 182.
[32] M. Motevalli, P. O'Brein, I.M. Watson, Polyhedron 15 (1996) 1865.
[33] T.J. Marks, J.A. Belot, C.J. Reedy, R.J. McNeely, D.B. Studebaker, D.A. Neumayer, C.L. Stern, J. Alloys Compd. 251 (1997) 243.
[34] S.R. Drake, M.B. Hursthouse, K.M.A. Malik, S.A.S. Miller, D.J. Otway, Inorg. Chem. 32 (1993) 4464.
[35] D.C. Bradley, H. Chudzynska, M.B. Hursthouse, M. Motevalli, Polyhedron 13 (1994) 7.
[36] I. Baxter, S.R. Drake, M.B. Hursthouse, K.M. Abdul Malik, J. McAleese, D.J. Otway, J.C. Plakatouras, Inorg. Chem. 34 (1995) 1384.
[37] G. Malandrino, R. Licata, F. Castelli, I.L. Fragalà, C. Benelli, Inorg. Chem. 34 (1995) 6233.
[38] G. Malandrino, O. Incontro, F. Castelli, I.L. Fragalà, C. Benelli, Chem. Mater. 8 (1996) 1292.
[39] S.J. Kang, Y.S. Jung, Y.S. Sohn, Bull. Korean Chem. Soc. 18 (1997) 75.
[40] S.J. Kang, Y.S. Jung, Y.S. Sohn, Bull. Korean Chem. Soc. 18 (1997) 266.
[41] G. Malandrino, C. Benelli, F. Castelli, I.L. Fragalà, Chem. Mater. 10 (1998) 3434.
[42] G. Malandrino, I.L. Fragalà, S. Aime, W. Dastrù, R. Gobetto, C. Benelli, J. Chem. Soc., Dalton Trans. (1998) 1509.
[43] K.D. Pollard, J.J. Vittal, G.P.A. Yap, R.J. Puddephatt, J. Chem. Soc., Dalton Trans. (1998) 1265.
[44] G. Malandrino, R. Lo Nigro, I.L. Fragalà, C. Benelli, Eur. J. Inorg. Chem. (2004) 500.
[45] J.H. Lee, Y.S. Jung, Y.S. Sohn, S.J. Kang, Bull. Korean Chem. Soc. 19 (1998) 231.
[46] S.J. Kang, Y.S. Jung, I.I.-H. Suh, Bull. Korean Chem. Soc. 20 (1999) 95.
[47] K.D. Pollard, H.A. Jenkins, R.J. Puddephatt, Chem. Mater. 12 (2000) 701.
[48] G. Malandrino, R. Lo Nigro, F. Castelli, I.L. Fragalà, C. Benelli, Chem. Vap. Depos. 6 (2000) 233.
[49] G. Malandrino, M. Bettinelli, A. Speghini, I.L. Fragalà, Eur. J. Inorg. Chem. (2001) 1039.
[50] W.J. Evans, D.G. Giarikos, M.A. Johnston, M.A. Greci, W.J. Ziller, J. Chem. Soc., Dalton Trans. 4 (2002) 520.
[51] S.J. Kang, S.K. Lee, Bull. Korean Chem. Soc. 24 (2003) 535.
[52] S.J. Kang, Bull. Korean Chem. Soc. 25 (2004) 1207.
[53] J. Plakatouras, C. Kavounis, C. Cardin, Acta Crystallogr. E 59 (2003) m838.

[54] R. Lo Nigro, R.G. Toro, G. Malandrino, I.L. Fragalà, P. Rossi, P. Dapporto, J. Electrochem. Soc. 151 (2004) F-206.
[55] G. Malandrino, I.L. Fragalà, Coord. Chem. Rev. 250 (2006) 1605.
[56] G. Malandrino, I.L. Fragalà, P. Scardi, Chem. Mater. 10 (1998) 3765.
[57] R. Lo Nigro, G. Malandrino, I.L. Fragalà, Chem. Mater. 13 (2001) 4402.
[58] G. Malandrino, L.M.S. Perdicaro, G. Condorelli, I.L. Fragalà, A. Cassinese, M. Barra, J. Mater. Chem. 15 (2005) 4718.
[59] G. Malandrino, A. Frassica, I.L. Fragalà, Chem. Vap. Depos. 3 (1997) 306.
[60] R. Lo Nigro, G. Malandrino, I.L. Fragala, M. Bettinelli, A. Speghini, J. Mater. Chem. 12 (2002) 2816.
[61] J.F. Roeder, B.C. Hendrix, F. Hintermaier, D.A. Desrochers, T.H. Baum, G. Bhandari, M. Chappuis, P.C. Van Buskirk, C. Dehm, E. Fritsch, N. Nagel, H. Wendt, H. Cerva, W. Honlein, C. Mazure, J. Eur. Ceram. Soc. 19 (1999) 1463.
[62] J.W. Park, J.T. Kim, S.M. Koo, C.G. Kim, Y.S. Kim, Polyhedron 19 (2000) 2547.
[63] S.R. Drake, M.B. Hursthouse, K.M. Abdul Malik, D.J. Otway, J. Chem. Soc., Dalton Trans. 19 (1993) 2883.
[64] S.R. Drake, S.A.S. Miller, M.B. Hursthouse, K.M.A. Malik, Polyhedron 12 (1993) 1621.
[65] H.K. Ryu, J.S. Heo, S.I. Cho, C. Chung, S.H. Moon, J. Electrochem. Soc. 147 (2000) 1130.
[66] D.L. Schulz, T.J. Marks, in: W.S. Rees Jr. (Ed.), CVD of Nonmetals, VCH, Weinheim, Germany, 1996, p. 71.
[67] G.G. Condorelli, S. Gennaro, I.L. Fragalà, Chem. Vap. Depos. 6 (2000) 185.
[68] C. Bedoya, G.G. Condorelli, A. Motta, A. Di Mauro, G. Anastasi, I.L. Fragalà, J.G. Lisoni, D. Wouters, Chem. Vap. Depos. 11 (2005) 269.
[69] C. Bedoya, G.G. Condorelli, A. Di Mauro, G. Anastasi, I.L. Fragalà, J.G. Lisoni, D. Wouters, Mater. Sci. Eng. B 118 (2005) 264.
[70] N.B. Colthup, L.H. Daly, S.E. Wiberley, Introduction to Infrared and Raman Spectroscopy, Academic Press, New York, 1964, p. 220.
[71] K. Nakamoto, Infrared and Raman Spectra of Inorganic and Coordination Compounds, John Wiley and Sons, New York, 1978.
[72] G.G. Condorelli, A. Baeri, I.L. Fragalà, Chem. Mater. 14 (2002) 4307.
[73] G.G. Condorelli, G. Anastasi, S. Giuffrida, I.L. Fragalà, in: M. Allendorf, F. Maury, F. Teyssandier (Eds.), Proceedings of the CVD XVI/EUROCVD 14, The Electrochemical Society, Pennington, NJ, 08, 2003, p. 112.
[74] I.M. Watson, Chem. Vap. Depos. 3 (1997) 9.
[75] G.G. Condorelli, A. Baeri, I.L. Fragalà, V. Lauretta, G. Smerlo, Mater. Sci. Semicon. Proc. 5 (2002) 135.
[76] D.S. Kil, J.M. Lee, J.S. Roh, Chem. Vap. Depos. 8 (2002) 195.
[77] H. Van Doveren, J.A.Th. Verhoeven, J. Elec. Spec. Related Phenom. 21 (1980) 265.
[78] R.P. Vasquez, J. Elec. Spec. Related Phenom. 56 (1991) 217.
[79] M.I. Sosulnikiv, Yu.A. Teterin, J. Elec. Spec. Related Phenom. 59 (1992) 111.
[80] Z. Liu, K. Xie, N. Wu, D. Shen, Z. Lin, Chinese Phys. Lett. 6 (1989) 261.
[81] S. Momose, R. Sahara, T. Nakamura, K. Tachibana, Jpn. J. Appl. Phys. 40 (2001) 5501.
[82] J.F. Moulder, W.F. Stickle, P.E. Sobol, K.D. Bomben, in: J. Chastain (Ed.), Handbook of X-ray Photoelectron Spectroscopy, Perkin-Elmer Corporation Physical Electronic Division, Minnesota, 1992.
[83] A.S. Lagutchev, K.J. Song, J.Y. Huang, P.K. Yang, T.J. Chuang, Chem. Phys. 226 (1998) 337.
[84] G.G. Condorelli, M.L. Hitchman, A.Y. Kovalgin, S.H. Shamlian, Proc.-Electrochem. Soc. 98 (23) (1998) 141.
[85] G.G. Condorelli, M.L. Hitchman, A.Y. Kovalgin, S.H. Shamlian, in: M.D. Allendorf, C. Bernard (Eds.), Chemical Vapor Deposition—Proceedings of the Fourteenth International Conference and EUROCVD-11, The Electrochemical Society, Pennington, NJ, 1997, 97-25, 901.
[86] V.V. Krisyuk, A.E. Turgambaeva, I.K. Igumenov, Chem. Vap. Depos. 4 (1998) 43.
[87] A.E. Turgambaeva, A.F. Bykov, I.K. Igumenov, J. Phys. IV France 5 (1995) 221.
[88] Y.S. Cho, S.I. Cho, H.K. Ryu, J.S. Heo, D.H. Lee, S.H. Moon, J. Electrochem. Soc. 150 (2003) 11.
[89] A. Baeri, G.G. Condorelli, I.L. Fragalà, in: P.C. McIntyre, S.R. Gilbert, Y. Miyasaka, R.W. Schwartz, D. Wouters (Eds.), Mater. Res. Soc. Symp. Proc., vol. 655, Materials Research Society, Warrendale, USA, 2001, C.C.5.
[90] G.S. Girolami, P.M. Jeffries, L.H. Dubois, J. Am. Chem. Soc. 115 (1993) 1015.
[91] J.E. Parmeter, J. Phys. Chem. 97 (1993) 11530.
[92] W. Lin, B.C. Wiegand, R.G. Nuzzo, G.S. Girolami, J. Am. Chem. Soc. 118 (1996) 5977.
[93] D. Lin-Vien, N.B. Colthup, W.G. Fateley, J.G. Grasselli, The Handbook of Infrared and Raman Characteristic Fraquencies of Organic Molecules, Academic Press, San Diego, 1991, 213.
[94] R.A. Nyquist, The Interpretation of Vapor-Phase Infrared Spectra, vol. 1, Stadtler Research Laboratories, Philadelphia, 1984, p. 9.
[95] C.B. Moore, G.C. Pimentel, J. Chem. Phys. 38 (1963) 2816.
[96] A.F. Bykov, A.E. Turgambaeva, I.K. Igumenov, P.P. Semyannikov, J. Phys. IV C5 (1995) 191.
[97] A.E. Turgambaeva, V.V. Krisyuk, A.F. Bykov, I.K. Igumenov, J. Phys. IV Pr8 (1999) 65.
[98] H. Harima, H. Ohnishi, K. Hanaoka, K. Tachibana, M. Kobayashi, S. Hoshinouchi, Jpn. J. Appl. Phys. 29 (1990) 1932.
[99] R. Ramesh, S. Aggarwal, O. Auciello, Mater. Sci. Eng. R-Rep 32 (2001) 191.
[100] R. Zambrano, Mater. Sci. Semicon. Proc. 5 (2002) 305.
[101] A.C. Jones, P.R. Chalker, J. Phys. D: Appl. Phys. 36 (2003) 80.
[102] H. Funakubo, N. Nukaga, K. Ishikawa, H. Kokubun, H. Machida, K. Shinozaki, N. Mizutani, Ferroelectrics 232 (1999) 123.
[103] T. Jimbo, H. Sano, Y. Takahasmi, H. Funakubo, E. Tokumitsu, H. Ishiwara, Jpn. J. Appl. Phys. 38 (1999) 6456.
[104] Y. Zhu, S.B. Desu, T. Li, S. Ramanathan, M. Nagata, J. Mater. Res. 12 (1997) 783.
[105] N.J. Seong, S.G. Yoon, S.S. Lee, Appl. Phys. Lett. 71 (1997) 81.
[106] G.G. Condorelli, A. Baeri, G. Anastasi, I.L. Fragalà, Mater. Sci. Semicon. Proc. 5 (2002) 167.
[107] G.G. Condorelli, M. Favazza, C. Bedoya, A. Baeri, G. Anastasi, R. Lo Nigro, N. Menou, Ch. Muller, J.G. Lisoni, D. Wouters, I.L. Fragalà, Chem. Mater. 18 (2006) 1016.
[108] C. Bedoya, G.G. Condorelli, G. Anastasi, A. Baeri, F. Scerra, I.L. Fragala, J.G. Lisoni, D. Wouters, Chem. Mater. 16 (2004) 3176.
[109] J. Liu, S. Zhang, C. Yang, L. Dai, J. Am. Ceram. Soc. 88 (2005) 85.
[110] T. Osaka, A. Sakakibara, T. Seki, S. Ono, I. Koiwa, A. Hashimoto, Jpn. J. Appl. Phys. Part 1 37 (1998) 597.
[111] M. Moert, G. Schindler, T. Mikolajick, N. Nagel, W. Hartner, C. Dehm, H. Kohlstedt, R. Waser, Appl. Surf. Sci. 249 (2005) 23.
[112] M. Viapiana, M. Schwitters, D.J. Wouters, H.E. Maes, O. Van der Biest, Mater. Sci. Eng. B 118 (2005) 34.
[113] W.C. Shin, K.J. Choi, S.G. Yoon, Thin Solid Films 409 (2002) 133.
[114] A. Cassinese, M. Barra, I. Fragalà, M. Kusunoki, G. Malandrino, T. Nakagawa, L.M.S. Perdicaro, K. Sato, S. Ohshima, R. Vaglio, Physica C 372–376 (2002) 500.
[115] M. Barra, A. Cassinese, I. Fragala, M. Kusunoki, G. Malandrino, T. Nakagawa, L.M.S. Perdicaro, K. Sato, S. Ohshima, R. Vaglio, Supercond. Sci. Technol. 15 (2002) 581.
[116] A. Cassinese, A. Andreone, E. Di Gennaro, G. Pica, R. Vaglio, G. Malandrino, L.M.S. Perdicaro, I.L. Fragalà, C. Granata, Supercond. Sci. Technol. 14 (2001) 406.
[117] G. Malandrino, A.M. Borzì, I.L. Fragalà, A. Andreone, A. Cassinese, G. Pica, J. Mater. Chem. 12 (2002) 3728.
[118] G. Malandrino, L.M.S. Perdicaro, G.G. Condorelli, I.L. Fragalà, A. Cassinese, A. Prigiobbo, Chem. Vap. Depos. 11 (2005) 381.
[119] K.N. Yang, Y. Dalichaouch, J.M. Ferreira, B.W. Lee, J.J. Neumeier, M.S. Torikachvili, H. Zhou, M.B. Maple, R.R. Hake, Solid State Commun. 63 (1987) 515.
[120] E.M. Engler, V.Y. Lee, A.I. Nazzal, R.B. Beyers, G. Lim, P.M. Grant, S.S.P. Parkin, M.L. Ramirez, J.E. Vazquez, R.J. Savoy, J. Am. Chem. Soc. 109 (1987) 2848.

[121] T. Rouillon, M. Hervieu, B. Domengès, B. Raveau, J. Solid State Chem. 103 (1993) 63.
[122] R.J. Cava, R.B. van Dover, B. Batlogg, E.A. Rietman, Phys. Rev. Lett. 58 (1987) 408.
[123] H. Müller-Buschbaum, Angew. Chem. Int. Ed. Engl. 28 (1989) 1472.
[124] X.F. Meng, F.S. Pierce, K.M. Wong, R.S. Amos, C.H. Xu, B.S. Deaver Jr., S.J. Poon, IEEE Trans. Magn. 27 (1991) 1638.
[125] A.A. Molodyk, A.R. Kaul, O.Yu. Gorbenko, M.A. Novojilov, I.E. Korsakov, G. Wahl, J. de Physique IV, Proceedings of the Twelfth European Conference on Chemical Vapour Deposition, vol. 2, 1999, p. 709.
[126] B. Han, D.A. Neumayer, D.L. Schulz, B.J. Hinds, T.J. Marks, H. Zhang, V.P. Dravid, Chem. Mater. 5 (1993) 14.
[127] M. Becht, T. Gerfin, K.H. Dahmen, Chem. Mater. 5 (1993) 137.
[128] C. Tian, Y. Du, S.-W. Chan, J. Vac. Sci. Technol. A 15 (1997) 85.
[129] H.J. Osten, J.P. Liu, H.J. Mussig, Appl. Phys. Lett. 80 (2002) 297.
[130] K. Tominaga, A. Shirayanagi, T. Takagi, M. Okada, Jpn. J. Appl. Phys. 32 (1993) 4082.
[131] A. Kingon, Nature 401 (1999) 658.
[132] S.R. Shannigrahi, S.-H. Lee, H.M. Jang, J. Mater. Res. 17 (2002) 1884.
[133] W. Tao, S.B. Desu, C.H. Peng, B. Dickerson, T.K. Li, C.L. Thio, J.J. Lee, W. Hendricks, Materials Research Society Symposium Proceedings—(Ferroelectric Thin Films IV), vol. 361, 1995, p. 319.
[134] S.D. Bu, B.S. Kang, B.H. Park, T.W. Noh, J. Korean Phys. Soc. 36 (2000) L9.
[135] T. Kijima, M. Ushikubo, H. Matsunaga, Jpn. J. Appl. Phys. 38 (1999) 127.
[136] G.Y. Ahn, S.I. Park, I.B. Shim, Y.S. Cho, C.S. Kim, Phys. Status Solidi B: Basic Res. 241 (2004) 1561.
[137] R. Von Helmolt, J. Wecker, B. Holzapfel, L. Schultz, K. Samwer, Phys. Rev. Lett. 71 (1993) 2331.
[138] T.K. Nath, R.A. Rao, D. Lavric, C.B. Eom, L. Wu, F. Tsui, Appl. Phys. Lett. 74 (1999) 1615.
[139] Y. Shiokawa, R. Amano, A. Nomura, M. Yagi, J. Radioanal. Nucl. Chem. 152 (1991) 373.
[140] A. Weber, H. Suhr, Mod. Phys. Lett. B 3 (1989) 1001.
[141] M. Nieminen, M. Putkonen, L. Niinistö, Appl. Surf. Sci. 174 (2001) 155.
[142] J.B. Cheng, A.D. Li, Q.Y. Shao, H.Q. Ling, D. Wu, Y. Wang, Y.J. Bao, M. Wang, Z.G. Liu, N.B. Ming, Appl. Surf. Sci. 233 (2004) 91.
[143] T. Nakamura, T. Nishimura, R. Tai, K. Tachibana, Mater. Sci. Eng. B 118 (2005) 253.
[144] C. Bedoya, G.G. Condorelli, S.T. Finocchiaro, A. Di Mauro, D. Atanasio, I.L. Fragalà, L. Cattaneo, S. Carella, Chem. Vap. Depos. 12 (2006) 46.
[145] H.C. Aspinall, J. Gaskell, P.A. Williams, A.C. Jones, P.R. Chalker, P.A. Marshall, L.M. Smith, G.W. Critchlow, Chem. Vap. Depos. 10 (2004) 13.
[146] A.M. De Asha, J.T.S. Critchley, R.M. Nix, Surf. Sci. 405 (1998) 201.
[147] B. Klingenberg, M.A. Vannice, Chem. Mater. 8 (1996) 2755.
[148] G. Malandrino, L.M.S. Perdicaro, I.L. Fragala, Chem. Vap. Depos. 12 (2006) 736.